

BREAKING RANK BOTTLENECKS IN KNOWLEDGE GRAPH EMBEDDINGS

Samy Badreddine^{1,2,3} Emile van Krieken^{4,*} Luciano Serafini^{2,3,*}

¹Sony AI ²Fondazione Bruno Kessler ³University of Trento ⁴Vrije universiteit Amsterdam
samy.badreddine@sony.com, e.van.krieken@vu.nl, luciano.serafini@fbk.eu

ABSTRACT

Many knowledge graph embedding (KGE) models for link prediction use powerful encoders. However, they often rely on a simple hidden vector-matrix multiplication to score subject-relation queries against candidate object entities. When the number of entities is larger than the model’s embedding dimension, which is often the case in practice by several orders of magnitude, we have a linear output layer with a *rank bottleneck*. Such bottlenecked layers limit model expressivity. We investigate both theoretically and empirically how rank bottlenecks affect KGEs. We find that, by limiting the set of feasible predictions, rank bottlenecks hurt the ranking accuracy and distribution fidelity of scores. Inspired by the language modelling literature, we propose KGE-MoS, a mixture-based output layer to break rank bottlenecks in many KGEs. Our experiments show that KGE-MoS improves ranking performance of KGE models on large-scale datasets at a low parameter cost.

1 INTRODUCTION

Knowledge graph completion (KGC) aims to predict missing triples in a knowledge graph (KG). For example, KGC models can find missing connections in a biomedical KG to reveal potential drug-disease associations (Himmelstein et al., 2017; Breit et al., 2020; Bonner et al., 2022), and are used as recommender systems in social networks or e-commerce (Hu et al., 2020). Most KGC models learn knowledge graph embeddings (KGEs) for entities and relations to obtain a score indicating what objects are likely for a given subject-relation pair (Nickel et al., 2015; Ji et al., 2022).

De facto KGE models score object entities by simply multiplying an embedding of the subject-relation query with the entity embedding matrix. This is the case for both bilinear or neural network approaches, even when they use powerful encoders like graph neural networks or language models (Ali et al., 2022). This vector-matrix multiplication linearly maps a hidden state of relatively low dimension (typically, 10^2 to 10^4) to a high-dimensional output space corresponding to the number of entities (typically, 10^4 to 10^6 for medium KGs, and up to 10^9 for industry-scale KGs (Sullivan, 2020)). Such linear output layers introduce low-rank constraints, often referred to as *rank bottlenecks*. Yang et al. (2017) showed that rank bottlenecks hurt language modelling (LM) perplexity.

However, rank bottlenecks in KGEs have not yet been studied, even though the number of KG entities is usually much larger than the vocabulary size in LM. We show that bottlenecking KGE models impacts the number of possible predictions by studying three prediction tasks (Figure 2). For instance, we use the graph factorisation literature to find an upper-bound on the rank required for exact KG factorisation, which grows for larger and denser graphs.

To break the rank bottleneck, we introduce KGE-MoS, which uses a mixture of softmaxes (MoS) (Yang et al., 2017) as a non-linear output layer. We evaluate KGE-MoS on five KGE models across knowledge graphs of increasing size. On the larger datasets, KGE-MoS improves both the ranking accuracy and probabilistic fit of probabilistic predictions at a lower parameter cost than simply increasing the KGE dimension.

Contributions. We (i) are the first to highlight the implications of rank bottlenecks on the three KGC prediction tasks in Figure 2 (Section 3). In Section 4, we (ii) provide sufficient dimensionality

*Equal supervision contribution.

Code available at github.com/sonyresearch/kgmos

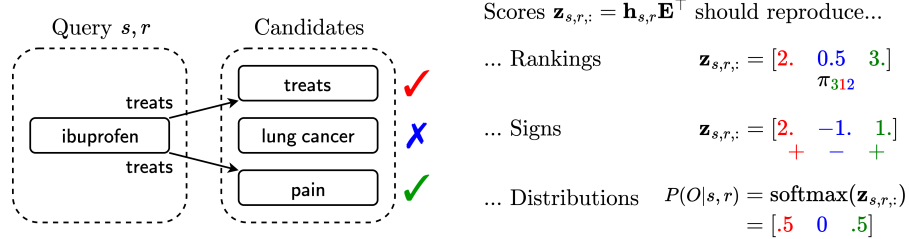


Figure 1: KGE models are used in various prediction tasks, each with their own expressivity needs.

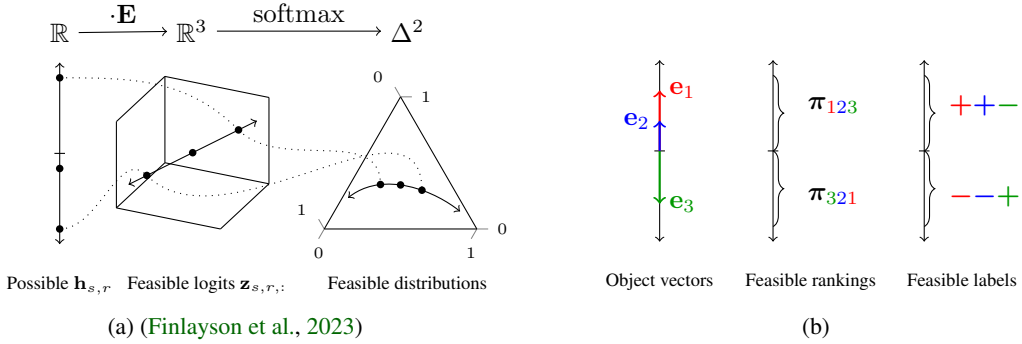


Figure 2: **Rank bottlenecks leave many score / ranking / sign-label reconstructions unfeasible** when $d < |\mathcal{E}| - 1$ (illustrated on a toy KGE, $d = 1, |\mathcal{E}| = 3$). (a) Projection of the hidden space of queries $(s, r, ?)$ by the matrix of object vectors \mathbf{E} . Logits lie in a 1D linear subspace. Probabilities after softmax lie in a 1D smooth manifold in the probability simplex, leaving all other points unfeasible. (b) Division of the hidden state space by object vectors \mathbf{e}_o into regions corresponding to different rankings / labels. Many configurations (e.g., π_{312} or $+-+$) are unfeasible.

conditions to perfectly break bottlenecks in some tasks and show that the task difficulty depends on the graph connectivity. We (iii) introduce KGE-MoS, a simple output layer that breaks rank bottlenecks and improves performance in large-scale benchmarks at a low parameter cost (Section 5).

2 KNOWLEDGE GRAPH COMPLETION

A knowledge graph (KG) is a common data structure for representing relational information. Let \mathcal{E} be a set of entities and \mathcal{R} a set of relations. A KG $\mathcal{G} = \{(s, r, o) \in \mathcal{E} \times \mathcal{R} \times \mathcal{E}\}$ is a set of triples where $s \in \mathcal{E}$ is a subject, $r \in \mathcal{R}$ is a relation, and $o \in \mathcal{E}$ is an object. In the knowledge graph completion (KGC) task, only some triples $\mathcal{G}_{\text{obs}} \subset \mathcal{G}$ are observed, and the task is to predict missing triples $\mathcal{G} \setminus \mathcal{G}_{\text{obs}}$ by predicting suitable objects for $(s, r, ?)$ queries. This is typically cast as a ranking problem where candidate objects are evaluated and ranked; correct answers are objects o such that $(s, r, o) \in \mathcal{G}$ (Nickel et al., 2015).

A knowledge graph embedding model (KGE) is a function $\phi : \mathcal{E} \times \mathcal{R} \times \mathcal{E} \rightarrow \mathbb{R}$ that assigns a score $z_{s,r,o}$ to each triple by embedding entities and relations.¹ Here, higher scores correspond to more likely triples. We use $\mathbf{e}_s, \mathbf{e}_o \in \mathbb{R}^d$ to denote the embeddings of subject and object entities respectively and $\mathbf{w}_r \in \mathbb{R}^{d_r}$ to denote the embedding of a relation r (often, $d_r = d$). Let $\mathbf{Z} \in \mathbb{R}^{|\mathcal{E}| \times |\mathcal{R}| \times |\mathcal{E}|}$ be the scores calculated for each triple arranged in a tensor. A KGE answers object prediction queries $(s, r, ?)$ by ordering entities by decreasing values of $\mathbf{z}_{s,r,:} \in \mathbb{R}^{|\mathcal{E}|}$.

¹We use $a, \mathbf{a}, \mathbf{A}, \mathbf{A}$ to denote scalars, vectors, matrices, and tensors respectively. See Appendix A for indexing and slicing notation.

2.1 OBJECT PREDICTION AS A HIDDEN VECTOR-MATRIX MULTIPLICATION

In this work, we focus on KGEs of the form

$$\phi(s, r, o) = \mathbf{h}_{s,r}^\top \mathbf{e}_o. \quad (1)$$

Here $\mathbf{h}_{s,r} \in \mathbb{R}^d$ is a representation of the subject and relation, and is typically the result of an encoding function $h(\mathbf{e}_s, \mathbf{w}_r)$. Most methods use a simple dot product with the object embedding \mathbf{e}_o to compute a score, enabling fast scoring for object prediction. Indeed, let $\mathbf{E} \in \mathbb{R}^{|\mathcal{E}| \times d}$ be the embeddings of all entities stacked in a matrix. The computation of scores for a fixed subject-relation pair (s, r) against all object entities becomes the efficient vector-matrix multiplication

$$\mathbf{z}_{s,r,:} = \mathbf{h}_{s,r} \mathbf{E}^\top. \quad (2)$$

This linear scoring against entity embeddings appears, as their name suggests, in all *bilinear models* such as RESCAL (Nickel et al., 2011), DISTMULT (Yang et al., 2014), COMPLEX (Trouillon et al., 2017), CP (Lacroix et al., 2018) and SIMPLE (Kazemi & Poole, 2018). The same can be derived for TUCKER (Balažević et al., 2019), a model that generalises all the above bilinear models as tensor decompositions. We detail how to rewrite each of these models as $\mathbf{h}_{s,r}^\top \mathbf{e}_o$ in Appendix D.1.

Neural KGEs are also of the form in Equation 1. They use a powerful neural encoder to embed subject and relation queries into a hidden state $\mathbf{h}_{s,r} = \text{NeuralNet}(\mathbf{e}_s, \mathbf{w}_r)$. Then they project the hidden state to logits in the object space using a simple linear layer, which recovers $\mathbf{h}_{s,r} \mathbf{E}^\top$. Neural encoders can be CNNs like CONVE (Dettmers et al., 2017; Balažević et al., 2018), graph convolutional networks like COMPGCN (Schlichtkrull et al., 2017; Vashisht et al., 2019), transformers (Galkin et al., 2020) or language models (Wang et al., 2022a; Choi et al., 2021; Wang et al., 2022b; Liu et al., 2022). See Appendix D.1 for details. In Section 7 we discuss additional KGC methods that do not score against the object embedding matrix and are outside the scope of this work.

2.2 OUTPUT FUNCTIONS AND TASK OBJECTIVES

The introduction of new KGEs went along with the introduction of new training methods and loss functions (Ruffinelli et al., 2020; Ali et al., 2022). For a detailed overview, see Appendix D.2. While KGEs are usually evaluated on ranking metrics, the choice of the output and corresponding loss functions often reflects different underlying task objectives. We introduce three such tasks of increasing difficulty.

Ranking reconstruction (RR) Given a query of the form $(s, r, ?)$, RR aims to assign scores such that each true target object o receives a higher score $z_{s,r,o}$ than any non-target object o' , i.e., $z_{s,r,o} > z_{s,r,o'}$ for all o and o' with $(s, r, o) \in \mathcal{G}$ and $(s, r, o') \notin \mathcal{G}$. RR is typically achieved with margin-based loss functions (Bordes et al., 2013; Yang et al., 2014).

Sign reconstruction (SR) For a query $(s, r, ?)$, sign reconstruction aims to learn a scoring function such that $z_{s,r,o} > 0$ if $(s, r, o) \in \mathcal{G}$, and $z_{s,r,o} < 0$ otherwise. This objective can be viewed as binary classification over triples (Trouillon et al., 2017; Dettmers et al., 2017; Pezeshkpour et al., 2020).

Distributional reconstruction (DR) Given a query $(s, r, ?)$, distributional reconstruction aims to recover uniform scores $z_{s,r,o} = \tau_+$ for all $(s, r, o) \in \mathcal{G}$ and $z_{s,r,o'} = \tau_-$ for all $(s, r, o') \notin \mathcal{G}$, with τ_+ a high score for true triples and $\tau_- < \tau_+$ a low score for negative triples. For example, $\tau_+ = 1$ and $\tau_- = 0$ corresponds to exact binary reconstruction. This can have a probabilistic interpretations, e.g. when $\tau_- \rightarrow -\infty$ for softmax layers, such that any larger τ_+ defines a uniform distribution over the true triples. Distributional reconstruction can be used for downstream reasoning. For example, Arakelyan et al. (2021; 2023) combine triple probabilities to answer complex queries, and Loconte et al. (2023) samples triples, which both require accurate data distributions.

We will say that a KGE is *expressive* for a task under a certain condition (typically, a dimensionality bound on its parameters) if there exists a parameter setting that satisfies the task objective under that condition. Notice that any model expressive for DR or SR is also expressive for RR. Moreover, by setting a decision threshold (e.g., $\frac{\tau_+ + \tau_-}{2}$), we can repurpose a model for DR to a model for SR.

Several KGEs are fully expressive, but the underlying theoretical conditions are impractical for real-world datasets. For example, TUCKER is fully expressive for any graph whenever $d_e = |\mathcal{E}|$ and $d_r = |\mathcal{R}|$ (Balažević et al., 2019), and COMPLEX achieves full expressivity with $d_e = d_r = |\mathcal{E}||\mathcal{R}|$ (Trouillon et al., 2017). Such requirements are unrealistic for larger datasets (e.g., $|\mathcal{E}| = 10^6$), making these theoretical guarantees not applicable in practice: typically, $d \ll |\mathcal{E}|$ by several orders of magnitude. This severely limits the expressivity of KGEs, as we discuss next.

3 RANK BOTTLENECKS IN KGEs...

In this section, we discuss the practical limitations in expressivity of bottlenecked KGEs in relation to each task objective defined above. We define a *bottlenecked KGE* as a KGE model that uses a vector-matrix multiplication for object prediction (see Section 2.1) and that has a dimension $d < |\mathcal{E}| - 1$. As the entity embedding matrix \mathbf{E} has rank at-most d , the score vector $\mathbf{z}_{s,r,:}$ is confined to a d -dimensional linear subspace of $\mathbb{R}^{|\mathcal{E}|}$. For a visual intuition, consider the bottlenecked KGE depicted in Figure 2a with $d=1$ and $|\mathcal{E}|=3$.

Bottlenecks are typically not an issue for intermediate layers in a neural network because repeated non-linear transformations can map the linear subspace to meaningful manifolds (e.g., as seen in autoencoders (Hinton & Zemel, 1993)). However, a bottleneck at the output layer of a model imposes more rigid limitations. We discuss each in the context of the task objectives previously introduced.

3.1 ... FOR SOLVING DISTRIBUTIONAL RECONSTRUCTION

To demonstrate the bottleneck in the predictive capability of a KGE, we compare the rank of the knowledge graph’s adjacency matrix to that of the KGE score matrix. Consider $\mathbf{Z} = \begin{bmatrix} \mathbf{z}_{1,1,:} \\ \vdots \\ \mathbf{z}_{|\mathcal{E}|,|\mathcal{R}|,:} \end{bmatrix} \in \mathbb{R}^{|\mathcal{E}||\mathcal{R}| \times |\mathcal{E}|}$, a view of the score tensor \mathcal{Z} rearranged to have subject-relation pairs on the first axis and objects on the second.² As $\mathbf{Z} = \mathbf{H}\mathbf{E}^\top$, where $\mathbf{H} = \begin{bmatrix} \mathbf{h}_{1,1} \\ \vdots \\ \mathbf{h}_{|\mathcal{E}|,|\mathcal{R}|} \end{bmatrix} \in \mathbb{R}^{|\mathcal{E}||\mathcal{R}| \times d}$ is the matrix of hidden states for each subject-relation pair, the rank of \mathbf{Z} is at most d . Consider now the ground-truth adjacency matrix of the graph $\mathbf{Y} \in \{0, 1\}^{|\mathcal{E}||\mathcal{R}| \times |\mathcal{E}|}$, where $y_{i,o}$ is 1 if o is an object for the subject-relation pair i and 0 otherwise. If \mathbf{Y} has a rank r greater than d , then the ground-truth relationships lie in a higher-dimensional space than the d -dimensional subspace spanned by the KGE scores. This leads to a trivial limitation in the model’s ability to accurately represent the true relationships.

Proposition 3.1 (DR bottleneck). *A bottlenecked KGE constrained to a low-rank d cannot represent the distributions in a true adjacency matrix $\mathbf{Y} \in \{0, 1\}^{|\mathcal{E}||\mathcal{R}| \times |\mathcal{E}|}$ with rank $r > d + 1$ perfectly.*

All proofs are in Appendix B. Notice that applying a softmax function on the scores, despite introducing non-linear interactions, still limits the feasible predictions in a rigid way. Softmax maps the d -dimensional linear subspace of scores to a smooth d -dimensional manifold within the corresponding probability simplex $\Delta^{|\mathcal{E}|-1}$ (see Figure 2a) (Finlayson et al., 2023). However, because softmax is log-linear, the manifold is rigidly constrained to certain shapes. Intuitively, this implies that class probability ratios on the manifold are linear on a logarithmic scale. Any ground truth that does not adhere to this constraint cannot be represented. We discuss this phenomenon called *softmax bottleneck* (Yang et al., 2017) in more detail in Appendix E.1.

3.2 ... FOR SOLVING RANKING RECONSTRUCTION

Next, we discuss how rank bottlenecks affect a model’s ability to correctly order potential objects, which is crucial for the usual KGC evaluation protocols. Borrowing the notation of Grivas et al. (2022), let π denote a permutation of objects. For example, in Figure 2b, the scores $\mathbf{z}_{s,r,:} = \mathbf{h}_{s,r}\mathbf{E}^\top = [-2 \ -0.5 \ 3.]$ would imply that we assign the query $\mathbf{h}_{s,r}$ the ranking π_{321} since $z_{s,r,3} > z_{s,r,2} > z_{s,r,1}$. Notice that activations like sigmoid or softmax preserve the ranking.

Theorem 3.2 (RR bottleneck). *A bottlenecked KGE with low-rank $d < |\mathcal{E}| - 1$ always has some unfeasible ranking configurations π , regardless of the learned input representations.*

²Formally, this would be the transposed mode-3 unfolding $\mathbf{Z}_{(3)}^\top$ of \mathcal{Z} , but we will denote it \mathbf{Z} for simplicity.

Table 1: Sufficient embedding dimension d_{SR} for exact sign reconstruction of $(s, r, ?)$ queries on different KGs including inverse relations. **The dimension scales with graph connectivity rather than simply the number of entities.**

Dataset	#Entities	#Rels	Out-degree		d_{SR}^+
			Avg	Max	
FB15k-237	14,541	237	3.83	4,364	8,729
Hetionet	45,158	24	21.66	15,036	30,073
ogbl-biokg	93,773	51	37.48	29,328	58,657
openbiolink	180,992	28	18.12	18,420	36,841

For example, in Figure 2b (our $d = 1, |\mathcal{E}| = 3$ toy model), we see that only the rankings π_{123} and π_{321} are feasible. If one query i has a different ground-truth ranking (e.g., π_{213}), then even the most powerful encoder for $\mathbf{h}_{s,r}$ cannot achieve the ground-truth ranking.

3.3 ... FOR SOLVING SIGN RECONSTRUCTION

We obtain a similar result for the SR task. Let $\mathbf{y} \in \{+, -\}^{|\mathcal{E}|}$ be the multi-label assignment of a query. For example, in Figure 2b, if we obtain the scores $\mathbf{z}_{s,r,:} = \mathbf{h}_{s,r} \mathbf{E}^\top = [-2 \ -0.5 \ 3]$, we assign the query \mathbf{h}_i the multi-label assignment $\mathbf{y} = [- \ - \ +]$.

Theorem 3.3 (SR bottleneck). *A bottlenecked KGE with low-rank $d < |\mathcal{E}|$ always has some unfeasible multi-label assignments configurations \mathbf{y} , regardless of the learned input representations.*

For example, in Figure 2b, we see that only the multi-label assignments $+++$ and $---$ are feasible. For any assignment \mathbf{y}_j that is different from these two, it is impossible to learn a representation \mathbf{h}_j such that the KGE classifies it correctly.

4 A SUFFICIENT BOUND FOR SIGN AND RANKING RECONSTRUCTION

While our theoretical results prove that bottlenecked KGEs cannot reconstruct some ranking and sign predictions, an important question remains: is there a bottlenecked model which, while unable to represent all possible results, can accurately represent the ground truths relevant to the knowledge graph? We address this by leveraging the graph’s structure to derive an upper bound on an embedding dimension d that is sufficient for accurate sign reconstruction.

Theorem 4.1. *Let $\mathbf{Y} \in \{0, 1\}^{|\mathcal{E}||\mathcal{R}|\times|\mathcal{E}|}$ be the representation of the KG with subject-relation pairs on the first axis and objects on the second. Let the sign function $s(x) = 1$ if $x > 0$ and $s(x) = 0$ otherwise. Then, \mathbf{Y} can be exactly decomposed as $\mathbf{Y} = s(\mathbf{H}\mathbf{E}^\top)$ where $\mathbf{H} \in \mathbb{R}^{|\mathcal{E}||\mathcal{R}|\times(2c+1)}$, $\mathbf{E} \in \mathbb{R}^{|\mathcal{E}|\times(2c+1)}$, and c is the maximum out-degree across all subject-relation pairs in the KG. The function $s(\cdot)$ is applied element-wise.*

The proof extends the reasoning of Theorem 6 of [Alon et al. \(1985\)](#) for bounding the sign rank of sparse matrices to rectangular bipartite matrices and is detailed in [Appendix B](#).

Corollary 4.2 (Sufficient rank for sign and ranking reconstruction). *For any KG with maximum out-degree c across subject-relation pairs, there exists a KGE with rank $d_{SR} = 2c + 1$ that achieves perfect sign reconstruction for queries $(s, r, ?)$. By extension, the KGE also achieves perfect ranking reconstruction, as positive scores for existing facts rank above negative scores for non-existing facts.*

[Table 1](#) presents the theoretical sufficient dimension $d_{SR} = 2c + 1$ for several KGs. In summary, more densely connected datasets are harder to fit in theory. This explains why a dataset like `ogbl-biokg`, despite having fewer nodes than `openbiolink`, is more challenging. We remark that the technique used to prove [Theorem 4.1](#) depends on an ordering of the entities, and the value $2c + 1$ is that of the *worst-case ordering*. In practice, the bound can be made tighter using better orderings (see [Fig. 4](#) in [Appendix](#)), but finding the optimal ordering is a hard problem and is dataset-specific.

Note that two practical questions remain. First, can existing KGEs, with their specific scoring functions, actually represent the factorisation technique described in [Theorem 4.1](#)? Second, even if they can, can this solution be efficiently learned through gradient-based optimisation in practice? We leave these for future work. Despite these challenges, this theoretical result provides a valuable guide for dimensionality choices and relating different dataset connectivities.

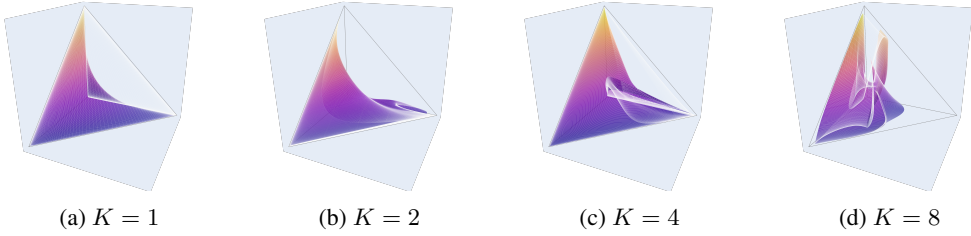


Figure 3: Feasible distributions of randomly initialised KGE-MoS output layers in a toy model ($d=2, |\mathcal{E}|=4$). The points are calculated for different inputs $\mathbf{h}_{s,r}$ while \mathbf{E} , ω_k and f_{θ_k} are fixed. **A higher number of softmaxes K has a higher representational power and can better fit arbitrary ground-truth $P^*(O|s,r)$.**

5 BREAKING RANK BOTTLENECKS WITH A MIXTURE OF SOFTMAXES

We now propose a solution to break rank bottlenecks in KGEs. A simple approach is to use a larger embedding dimension d to reflect the graph size or, according to the bound of Theorem 4, its connectivity. However, this quickly becomes impractical for large graphs. Instead, we adapt the *Mixture of Softmaxes* (MoS) layer proposed in language modelling (Yang et al., 2017) to KGEs.

Let O be a random variable over the objects. KGE models use the softmax for object prediction $(s, r, ?)$ to model a categorical distribution $P(O|s,r) = \text{softmax}(\mathbf{h}_{s,r}\mathbf{E}^\top) \in \Delta^{|\mathcal{E}|-1}$, where $\Delta^{|\mathcal{E}|-1}$ is the probability simplex over the objects. This distribution should align with the data distribution (labels of the corresponding triples, normalised to sum to 1). Although softmax is traditionally used for predicting a single correct class, it is often repurposed for multi-label scenarios by retrieving top- k entries, for ranking likely completions (RR) and for modelling generative distributions (DR). Extensive benchmarking efforts have shown that training KGEs with softmax and CE loss leads to the best results (Ruffinelli et al., 2020; Ali et al., 2022).

As shown in Sections 3.1 and 3.2, a bottlenecked KGE model with a softmax activation cannot represent all possible distributions and rankings over the objects. We propose using a KGE-MoS layer, which is a mixture of K softmaxes, to break these rank bottlenecks. Specifically,

$$P(O|s,r) = \sum_{k=1}^K \pi_k(\mathbf{h}_{s,r}) \text{softmax}(f_k(\mathbf{h}_{s,r})\mathbf{E}^\top), \quad \sum_{k=1}^K \pi_k(\mathbf{h}_{s,r}) = 1, \quad (3)$$

where $\pi_k(\mathbf{h}_{s,r}) \in [0, 1]$ is the prior or mixture weight of the k -th component and $f_k(\mathbf{h}_{s,r}) \in \mathbb{R}^d$ is the k -th context vector associated with the input (s, r) . The prior is parameterised as $\pi_k(\mathbf{h}_{s,r}) = \exp \mathbf{h}_{s,r}^\top \omega_k / \sum_{k'} \exp \mathbf{h}_{s,r}^\top \omega_{k'}$ with $\omega_k \in \mathbb{R}^d$. The context vector $f_k(\mathbf{h}_{s,r})$ is obtained by mapping the hidden state with a component-specific projection with parameters θ_k . In this work, we model each f_k with a two-layer MLP. Notice that only the parameters θ_k and ω_k are component-specific, resulting in a low additional parameter cost. $\mathbf{E} \in \mathbb{R}^{|\mathcal{E}| \times d}$ is shared.

The weighted combination of softmaxes is a non-linear transformation of logits which, while not increasing the dimension of the manifold spanned by the KGE, allows for a more complex set of distributions to be represented (see Figure 3). A more algebraic perspective considers the empirical log-probability matrix of the KGE predictions (see Appendix E.1), which resides in a linear subspace with $K = 1$ softmax and in a non-linear subspace when $K > 1$ (Yang et al., 2017). In Appendix F.4.2, we confirm that KGE-MoS breaks the rank bottleneck by measuring the rank of this log-probability matrix for $K = 1$ softmax and $K > 1$ softmaxes on actual KGs.

KGE-MoS is a drop-in solution that can be applied to any KGE method presented in Section 2.1 (e.g., CONVE). Simply replacing their output layer results in a high-rank variant (e.g., CONVE-MoS) for a low parameter cost $O(Kd + K|\theta_k|)$, which in our case gives $O(Kd^2)$. In contrast, increasing the dimension of the KGE by a factor d_{inc} has a cost $O(d_{\text{inc}}(|\mathcal{E}| + |\mathcal{R}|))$ which is usually less scalable as $|\mathcal{E}| \gg Kd$. Notice that while bilinear models (e.g., DISTMULT) can perform subject prediction $(?, r, o)$ scalably as a vector-matrix multiplication, their augmentations (e.g., DISTMULT-MoS) cannot, and must rely on inverse relations $(o, r^{-1}, ?)$. We discuss this in Appendix C.

6 EXPERIMENTS

We aim to answer the following research questions: **(RQ1)** “How does the performance of models with the proposed KGE-MoS output layer compare to bottlenecked KGE models?” **(RQ2)** “How does increasing the embedding size, as a simple alternative, compare to KGE-MoS in performance?”

Datasets We evaluate the performance of KGE models on the following standard datasets for link prediction: FB15k-237 (Toutanova & Chen, 2015), Hetionet (Himmelstein et al., 2017), ogbl-biokg (Hu et al., 2020), and openbiolink (Breit et al., 2020). FB15k-237 is a commonly used KGC benchmark, but its size is relatively small compared to modern KGs. We choose the other datasets for their larger sizes, as we expect rank bottlenecks to be more impactful in larger graphs due to our theoretical results. See Appendix F.1 for details and statistics.

Models For the baseline KGE models, we use DISTMULT (Yang et al., 2014), COMPLEX (Trouillon et al., 2017), RESCAL (Nickel et al., 2011) and CONVE (Dettmers et al., 2017), each trained using a softmax output layer and inverse relations for subject prediction, as they are standard choices for link prediction (Ruffinelli et al., 2020; Ali et al., 2022). We also include COMPGCN (Vashishth et al., 2019) to study a more expressive neural encoder. We use the best-performing hyperparameters found by Ruffinelli et al. (2020) (see Appendix F.3). We compare the baselines with their high-rank variants DISTMULT-MoS, RESCAL-MoS, etc., where we replace the softmax output layer with the KGE-MoS output layer using $K = 4$ softmaxes. We train each model with bottlenecks at $d = 200$ and $d = 1000$, except for COMPLEX where we halve the dimensions for comparability as the model has a bottleneck of $2d$ (see Appendix D.1). For COMPGCN we only evaluate in the low-dimensional regime due to computational constraints. The hyperparameters for the KGE-MoS output layer are found with a random search on ogbl-biokg and detailed in Appendix F.3.

Metrics As usual (Nickel et al., 2015; Ruffinelli et al., 2020; Ali et al., 2022), we assess the models for predicting object queries $(s, r, ?)$ and subject queries $(?, r, o)$ using filtered mean reciprocal rank (MRR) (see Appendix F.2). We measure the distributional fidelity of the models using the negative log likelihood (NLL) of the model predictions on the test set. Whereas previous work (Locoste et al., 2023) directly reports the NLL, we introduce a *filtered NLL* metric which more accurately reflects the predictive performance of a model for KGC. This prevents penalising models that assign low total probability mass outside training triples. See Appendix F.2 for more details.

6.1 RESULTS

Our results are reported in Table 2. We ran each of the twelve models (six models \times two embedding sizes) three times per dataset with different initialisations for statistical significance.

(RQ1) On the three larger datasets, the best performing models are consistently KGE-MoS models in both low and high dimensional regimes. The best performing model are often DISTMULT-MoS or COMPLEX-MoS, hinting that a simple encoder for the subject-relation with an elaborate output layer for the objects might be the most effective approach. In contrast, on the smallest dataset FB15k-237, KGE-MoS does not improve or sometimes even hurts the performance of bottlenecked KGE models, likely due to overfitting. In fact, the best KGE at $d = 200$ (CONVE) performs almost equally to the best KGE at $d = 1000$ (DISTMULT), hinting that rank bottlenecks are not critical in small-scale datasets. We confirm this in Appendix F.4, where we report similar results on WN18RR, a dataset with even lower connectivity than FB15k-237.

(RQ2) Comparing models across dimensions, we find that, **on the three larger datasets, KGE-MoS at $d = 200$ obtains almost as strong performance as the bottlenecked baselines at $d = 1000$.** Still, the performance increase of KGE-MoS models is larger at $d = 1000$ than at $d = 200$, suggesting that increasing embedding dimension not only helps with bottlenecks, it also unlocks input representation power. In an additional experiment in Appendix F.4.4, we tried to evaluate bottlenecked KGEs in larger datasets at $d = 5000$, to push the KGE dimension until bottlenecks do not matter. We find that **naively increasing embedding size past some high value requires compromising the training batch size and hurts performance.** This contrasts with the efficiency of KGE-MoS and its low parameter cost.

Table 2: **KGE-MoS improves performance and probabilistic fit of KGEs on large-scale datasets.** Average NLL \downarrow and MRR \uparrow . Standard deviations and Hits@ metrics are reported in Appendix F.4. Best results per dataset and dimension in **bold**. We also report the average improvement in NLL and MRR (mixture vs regular) per dataset and dimension. $*$ indicates statistical significance at $p < 0.05$ in a Wilcoxon signed-rank test pairing each model with its mixture variant.

MODEL	FB15k-237			HETIONET			OGBL-BIOKG			OPENBIOLINK		
	NLL	MRR	PARAM	NLL	MRR	PARAM	NLL	MRR	PARAM	NLL	MRR	PARAM
$d = 200$												
DISTMULT	4.74	.304	3.0M	6.10	.250	9.0M	4.83	.792	18.8M	5.14	.302	36.2M
DISTMULT-MoS	4.65	.306	3.3M	5.83	.277	9.4M	4.65	.792	19.1M	5.03	.314	36.5M
COMPLEX [†]	4.74	.303	3.0M	6.10	.249	9.0M	4.83	.792	18.8M	5.13	.301	36.2M
COMPLEX-MoS [†]	4.71	.301	3.3M	5.85	.269	9.4M	4.65	.793	19.1M	5.06	.313	36.5M
RESCAL	4.79	.258	21.9M	6.13	.219	10.9M	4.89	.763	22.8M	5.16	.303	38.4M
RESCAL-MoS	4.65	.318	22.2M	5.87	.274	11.3M	4.70	.780	23.2M	5.04	.323	38.8M
CONVE	4.48	.321	5.1M	6.03	.252	11.1M	4.94	.782	20.8M	5.28	.286	38.3M
CONVE-MoS	4.57	.311	5.4M	5.92	.263	11.4M	4.77	.768	21.2M	5.10	.304	38.6M
COMPGCN [‡]	4.80	.300	1.6M	5.95	.260	4.7M	5.11	.749	9.5M	5.43	.263	18.3M
COMPGCN-MoS [‡]	4.86	.310	2.0M	5.86	.266	5.0M	4.96	.744	9.6M	5.43	.274	18.3M
avg -MOS delta	-.02	.006		*-.19	*.022		*-.17	.000		*-.12	*.015	
$d = 1000$												
DISTMULT	4.56	.331	15.0M	6.04	.288	45.2M	4.89	.801	93.9M	5.17	.316	181.0M
DISTMULT-MoS	4.72	.311	23.0M	5.76	.312	53.2M	4.34	.837	101.9M	4.89	.347	189.0M
COMPLEX [†]	4.71	.317	15.0M	5.99	.292	45.2M	4.86	.806	93.9M	5.12	.322	181.0M
COMPLEX-MoS [†]	4.64	.314	23.0M	5.78	.303	53.2M	4.39	.836	101.9M	4.87	.345	189.0M
RESCAL	4.64	.307	488.5M	5.93	.243	93.1M	4.74	.799	195.8M	5.03	.328	237.0M
RESCAL-MoS	4.63	.325	496.5M	5.87	.300	101.2M	4.42	.824	203.8M	5.00	.328	245.0M
CONVE	4.65	.301	70.1M	6.06	.262	100.3M	4.93	.807	149.0M	5.24	.308	236.2M
CONVE-MoS	4.69	.316	78.2M	5.71	.313	108.3M	4.43	.817	157.0M	4.91	.336	244.2M
avg -MOS delta	.02	.002		*-.23	*.035		*-.43	*.024		*-.22	*.021	

[†] Results for COMPLEX use halved $d = 100$ and $d = 500$. It has real and imaginary parameters, leading to a rank bottleneck of $2d$.

[‡] Results for COMPGCN use $d = 100$ on ogbl-biokg and $d = 50$ on openbiolink due to computational constraints.

Table 3: MRR and NLL on ogbl-biokg at $d = 1000$ with different numbers of softmaxes.

MODEL	#SOFTMAXES	NLL \downarrow	MRR \uparrow
DISTMULT	1	4.89 \pm 0.02	.801 \pm 0.002
DISTMULT-MoS	1	4.42 \pm 0.01	.821 \pm 0.000
DISTMULT-MoS	2	4.37 \pm 0.01	.831 \pm 0.001
DISTMULT-MoS	4	4.34 \pm 0.01	.837 \pm 0.001
DISTMULT-MoS	8	4.33\pm0.00	.841\pm0.001

Mixture ablation Next, we run an ablation on the number of softmaxes used in KGE-MoS. We use ogbl-biokg, as Section 4 suggests it to be the most challenging dataset for bottlenecks due to its high connectivity, and DISTMULT-MoS, the best performing model. Table 3 details the results, with each value averaged over three runs. Increasing the number of softmaxes consistently leads to better performance, which is explainable by the larger representational power at each level (Figure 3). Notice that DISTMULT-MoS at $K = 1$, which does not mix any softmaxes and is a bottlenecked baseline, outperforms DISTMULT. This result can only be due to the projection layer f_{θ_k} . DISTMULT cannot represent asymmetric relations (i.e., $\phi(s, r, o) = \phi(o, r, s)$) (Trouillon et al., 2017; Lacroix et al., 2018). The projection layer adds asymmetry, which solves the limitation and likely explains the improvement.

Computational cost While KGE-MoS has a marginal parameter cost, its computational cost is higher than that of a regular softmax layer. On openbiolink, the dataset with the largest output layer, we find that KGE-MoS at $K = 4$ is between 1.69 and 2.75 times slower than its bottlenecked baseline for a training step. The largest difference is recorded for DISTMULT and DISTMULT-MoS, since DISTMULT is a very simple model. Still, we notice that the number of softmaxes has a negligible impact on inference time. See Table 7 for details. We find most of the overhead is due to the computation of the projections $f_{\theta_k}(\mathbf{h}_{s,r})$. Therefore, if inference time is a concern, this can be mitigated by using a more efficient projection layer.

7 RELATED WORK

Rank bottlenecks Rank bottlenecks in output layers of neural networks were first studied in *softmax models* for language modelling (Yang et al., 2017). If the task is to predict a single best completion for a query, low-rank constraints are less problematic (Grivas et al., 2022). However, to predict a distribution over the vocabulary or all plausible completions of a prompt, rank bottlenecks severely limit the expressivity of the model. Yang et al. (2017) proposed a mixture of softmaxes as an output layer to break the rank bottleneck in language modelling. Yang et al. (2019) proposed a variant, more scalable mixture model, whereas Kanai et al. (2018); Ganea et al. (2019) proposed alternative non-linearities. Grivas et al. (2023) explored rank bottlenecks in clinical and image *multi-label classification* and proposed a discrete Fourier transform output layer to guarantee a minimum number of label combinations to be feasible. To the best of our knowledge, we are the first to study rank bottlenecks in the context of KGEs. Earlier works (Trouillon et al., 2017; Kazemi & Poole, 2018; Balažević et al., 2019) have given theoretical guarantees on the expressivity of KGE models, but the provided conditions on the embedding dimension (e.g., $d \geq |\mathcal{E}|$) are unrealistic for large datasets. Recent work (Arakelyan et al., 2021; 2023; Harzli et al., 2023; Gregucci et al., 2024) has also emphasised the importance and lack of well-distributed output scores of KGE models for downstream reasoning.

Object prediction without vector-matrix multiplication Next, we discuss alternative approaches to KGC that do not use a score function as described in Section 2.1 and are outside the scope of this work. *Translation- and rotation-based KGEs* (Bordes et al., 2013; Wang et al., 2014; Lin et al., 2015; Sun et al., 2019) score objects using distance metrics like $\|\mathbf{h}_{s,r} - \mathbf{e}_o\|$, where relations act as geometric transformations (translations or rotations) in vector space. Translational models are interpretable and fast but are generally not fully expressive (Kazemi & Poole, 2018; Abboud et al., 2020). *Region-based KGEs* (Abboud et al., 2020; Pavlović & Sallinger, 2022) replace vector translations with geometric containment. Entities are embedded as points and relations as boxes. Scoring is based on whether objects lie within the box defined by the subject and relation. These KGEs prioritise spatial interpretability and complex inference patterns (e.g., hierarchical rule injection). They can be shown to be fully expressive, but with large dimension bounds – e.g., $d \geq |\mathcal{E}||\mathcal{R}|$ (Pavlović & Sallinger, 2022) – which are impractical for large datasets. Their performance in a low-dimensional regime should be studied further to investigate other forms of bottlenecks. Finally, some models for KGC do not use a traditional KGE-based scoring function, but have more complex reasoning mechanisms like *graph sampling* (Bi et al., 2022) or *path-based reasoning* (Das et al., 2017; Zhu et al., 2021), which are not subject to our analysis. However, some of these models internally use regular KGE scoring functions (Zhu et al., 2021), so our results could partially be extended to them.

8 CONCLUSIONS

In this paper, we showed that rank bottlenecks are a fundamental limitation of many standard KGE models. We demonstrated how these bottlenecks limit the model’s expressivity, affecting ranking accuracy and the distributional fidelity of probabilistic predictions. To address this, we introduced KGE-MoS, a mixture-based output layer that effectively breaks rank bottlenecks. Our experiments show that KGE-MoS improves both performance and distributional fidelity of KGEs when working with large KGs, at a low parameter cost. Our findings suggest that exploring other solutions for breaking rank bottlenecks is a promising avenue for advancing KGEs.

Limitations Our bound on a sufficient embedding dimension for sign and ranking reconstruction highlights that the task difficulty depends on the graph connectivity. More work is needed to provide tighter bounds and understand whether these solutions are representable by current KGEs. Secondly, while KGE-MoS improves performance on larger datasets, the computational cost during inference is higher than standard KGE models. This can be mitigated by using more efficient projection layers. Finally, we did not evaluate KGE-MoS on knowledge graphs with more than millions of entities. Exploring its performance and scalability in settings with significantly larger KGs remains an important avenue for future research.

ACKNOWLEDGEMENTS

Emile van Krieken was funded by ELIAI (The Edinburgh Laboratory for Integrated Artificial Intelligence), EPSRC (grant no. EP/W002876/1). Luciano Serafini was funded by the NRRP project Future AI Research (FAIR - PE00000013) under the NRRP MUR program, funded by NextGenerationEU. We would like to express our gratitude to Andreas Grivas, Pablo Sanchez Martin, Samuel Cognolato, Tarek R. Besold, Antonio Vergari, and Pasquale Minervini for fruitful discussions during the writing of this paper.

REFERENCES

Ralph Abboud, İsmail İlkan Ceylan, Thomas Lukasiewicz, and Tommaso Salvatori. BoxE: A Box Embedding Model for Knowledge Base Completion, 2020. URL <https://arxiv.org/abs/2007.06267>. Version Number: 2.

Mehdi Ali, Max Berrendorf, Charles Tapley Hoyt, Laurent Vermue, Sahand Sharifzadeh, Volker Tresp, and Jens Lehmann. PyKEEN 1.0: A Python Library for Training and Evaluating Knowledge Graph Embeddings, 2020. URL <https://arxiv.org/abs/2007.14175>. Version Number: 2.

Mehdi Ali, Max Berrendorf, Charles Tapley Hoyt, Laurent Vermue, Mikhail Galkin, Sahand Sharifzadeh, Asja Fischer, Volker Tresp, and Jens Lehmann. Bringing Light Into the Dark: A Large-Scale Evaluation of Knowledge Graph Embedding Models Under a Unified Framework. *IEEE Transactions on Pattern Analysis and Machine Intelligence*, 44(12):8825–8845, December 2022. ISSN 0162-8828, 2160-9292, 1939-3539. doi:10.1109/TPAMI.2021.3124805. URL <https://ieeexplore.ieee.org/document/9601281/>.

N. Alon, P. Frankl, and V. Rodl. Geometrical realization of set systems and probabilistic communication complexity. In *26th Annual Symposium on Foundations of Computer Science (sfcs 1985)*, pp. 277–280, October 1985. doi:10.1109/SFCS.1985.30. URL <https://ieeexplore.ieee.org/document/4568151>. ISSN: 0272-5428.

Erik Arakelyan, Daniel Daza, Pasquale Minervini, and Michael Cochez. Complex Query Answering with Neural Link Predictors. *arXiv:2011.03459 [cs]*, January 2021. URL <http://arxiv.org/abs/2011.03459>. arXiv: 2011.03459.

Erik Arakelyan, Pasquale Minervini, Daniel Daza, Michael Cochez, and Isabelle Augenstein. Adapting Neural Link Predictors for Data-Efficient Complex Query Answering, 2023. URL <https://arxiv.org/abs/2301.12313>. Version Number: 3.

Ivana Balažević, Carl Allen, and Timothy M. Hospedales. Hypernetwork Knowledge Graph Embeddings. 2018. doi:10.48550/ARXIV.1808.07018. URL <https://arxiv.org/abs/1808.07018>. Publisher: arXiv Version Number: 5.

Ivana Balažević, Carl Allen, and Timothy M. Hospedales. TuckER: Tensor Factorization for Knowledge Graph Completion. 2019. doi:10.48550/ARXIV.1901.09590. URL <https://arxiv.org/abs/1901.09590>. Publisher: arXiv Version Number: 2.

Zhen Bi, Siyuan Cheng, Jing Chen, Xiaozhuan Liang, Feiyu Xiong, and Ningyu Zhang. Relphomer: Relational Graph Transformer for Knowledge Graph Representations. 2022. doi:10.48550/ARXIV.2205.10852. URL <https://arxiv.org/abs/2205.10852>. Publisher: arXiv Version Number: 6.

Stephen Bonner, Ian P. Barrett, Cheng Ye, Rowan Swiers, Ola Engkvist, Charles Tapley Hoyt, and William L. Hamilton. Understanding the performance of knowledge graph embeddings in drug discovery. *Artificial Intelligence in the Life Sciences*, 2:100036, December 2022. ISSN 26673185. doi:10.1016/j.ailsc.2022.100036. URL <https://linkinghub.elsevier.com/retrieve/pii/S2667318522000071>.

Antoine Bordes, Nicolas Usunier, Alberto Garcia-Duran, Jason Weston, and Oksana Yakhnenko. Translating Embeddings for Modeling Multi-relational Data. In *Advances in Neural Information Processing Systems*, volume 26. Curran Associates, Inc., 2013. URL https://papers.nips.cc/paper_files/paper/2013/hash/1cecc7a77928ca8133fa24680a88d2f9-Abstract.html.

Anna Breit, Simon Ott, Asan Agibetov, and Matthias Samwald. OpenBioLink: a benchmarking framework for large-scale biomedical link prediction. *Bioinformatics*, 36(13):4097–4098, July 2020. ISSN 1367-4803, 1367-4811. doi:10.1093/bioinformatics/btaa274. URL <https://academic.oup.com/bioinformatics/article/36/13/4097/5825726>.

Sudhanshu Chanpuriya, Cameron Musco, Konstantinos Sotiropoulos, and Charalampos E. Tsourakakis. Node Embeddings and Exact Low-Rank Representations of Complex Networks, 2020. URL <https://arxiv.org/abs/2006.05592>. Version Number: 2.

Bonggeun Choi, Daesik Jang, and Youngjoong Ko. MEM-KGC: Masked Entity Model for Knowledge Graph Completion With Pre-Trained Language Model. *IEEE Access*, 9:132025–132032, 2021. ISSN 2169-3536. doi:10.1109/ACCESS.2021.3113329. URL <https://ieeexplore.ieee.org/document/9540703/>.

Andrzej Cichocki, Danilo Mandic, Lieven De Lathauwer, Guoxu Zhou, Qibin Zhao, Cesar Caiafa, and Huy Anh Phan. Tensor Decompositions for Signal Processing Applications: From two-way to multiway component analysis. *IEEE Signal Processing Magazine*, 32(2):145–163, March 2015. ISSN 1053-5888. doi:10.1109/MSP.2013.2297439. URL <http://ieeexplore.ieee.org/document/7038247/>.

Thomas M. Cover. Geometrical and Statistical Properties of Systems of Linear Inequalities with Applications in Pattern Recognition. *IEEE Transactions on Electronic Computers*, EC-14(3): 326–334, June 1965. ISSN 0367-7508. doi:10.1109/PGEC.1965.264137. URL <https://ieeexplore.ieee.org/document/4038449>.

Thomas M. Cover. The Number of Linearly Inducible Orderings of Points in d-Space. *SIAM Journal on Applied Mathematics*, 15(2):434–439, 1967. ISSN 0036-1399. URL <https://www.jstor.org/stable/2946294>. Publisher: Society for Industrial and Applied Mathematics.

Rajarshi Das, Shehzaad Dhuliawala, Manzil Zaheer, Luke Vilnis, Ishan Durugkar, Akshay Krishnamurthy, Alex Smola, and Andrew McCallum. Go for a Walk and Arrive at the Answer: Reasoning Over Paths in Knowledge Bases using Reinforcement Learning, 2017. URL <https://arxiv.org/abs/1711.05851>. Version Number: 2.

Tim Dettmers, Pasquale Minervini, Pontus Stenetorp, and Sebastian Riedel. Convolutional 2D Knowledge Graph Embeddings, 2017. URL <https://arxiv.org/abs/1707.01476>. Version Number: 6.

Matthew Finlayson, John Hewitt, Alexander Koller, Swabha Swayamdipta, and Ashish Sabharwal. Closing the Curious Case of Neural Text Degeneration, 2023. URL <https://arxiv.org/abs/2310.01693>. Version Number: 1.

Mikhail Galkin, Priyansh Trivedi, Gaurav Maheshwari, Ricardo Usbeck, and Jens Lehmann. Message Passing for Hyper-Relational Knowledge Graphs, 2020. URL <https://arxiv.org/abs/2009.10847>. Version Number: 1.

Octavian-Eugen Ganea, Sylvain Gelly, Gary Bécigneul, and Aliaksei Severyn. Breaking the Softmax Bottleneck via Learnable Monotonic Pointwise Non-linearities. 2019. doi:10.48550/ARXIV.1902.08077. URL <https://arxiv.org/abs/1902.08077>. Publisher: arXiv Version Number: 2.

Xavier Glorot and Yoshua Bengio. Understanding the difficulty of training deep feedforward neural networks. In *Proceedings of the Thirteenth International Conference on Artificial Intelligence and Statistics*, pp. 249–256. JMLR Workshop and Conference Proceedings, March 2010. URL <https://proceedings.mlr.press/v9/glorot10a.html>. ISSN: 1938-7228.

I. J Good and T. N Tideman. Stirling numbers and a geometric structure from voting theory. *Journal of Combinatorial Theory, Series A*, 23(1):34–45, July 1977. ISSN 0097-3165. doi:10.1016/0097-3165(77)90077-2. URL <https://www.sciencedirect.com/science/article/pii/0097316577900772>.

Cosimo Gregucci, Bo Xiong, Daniel Hernandez, Lorenzo Loconte, Pasquale Minervini, Steffen Staab, and Antonio Vergari. Is Complex Query Answering Really Complex?, 2024. URL <https://arxiv.org/abs/2410.12537>. Version Number: 2.

Andreas Grivas, Nikolay Bogoychev, and Adam Lopez. Low-Rank Softmax Can Have Unargmaxable Classes in Theory but Rarely in Practice, 2022. URL <https://arxiv.org/abs/2203.06462>. Version Number: 2.

Andreas Grivas, Antonio Vergari, and Adam Lopez. Taming the Sigmoid Bottleneck: Provably Argmaxable Sparse Multi-Label Classification, 2023. URL <https://arxiv.org/abs/2310.10443>. Version Number: 2.

Ouns El Harzli, Samy Badreddine, and Tarek R. Besold. What's Wrong with Gradient-based Complex Query Answering? 2023. URL <https://www.semanticscholar.org/paper/What's-Wrong-with-Gradient-based-Complex-Query-Harzli-Badreddine/404367d05dcd14167aa75ef6e3fdb203279dace>.

Daniel Scott Himmelstein, Antoine Lizee, Christine Hessler, Leo Brueggeman, Sabrina L Chen, Dexter Hadley, Ari Green, Pouya Khankhanian, and Sergio E Baranzini. Systematic integration of biomedical knowledge prioritizes drugs for repurposing. *eLife*, 6:e26726, September 2017. ISSN 2050-084X. doi:10.7554/eLife.26726. URL <https://elifesciences.org/articles/26726>.

Geoffrey E Hinton and Richard Zemel. Autoencoders, Minimum Description Length and Helmholtz Free Energy. In *Advances in Neural Information Processing Systems*, volume 6. Morgan-Kaufmann, 1993. URL https://proceedings.neurips.cc/paper_files/paper/1993/hash/9e3cfc48eccf81a0d57663e129aef3cb-Abstract.html.

Weihua Hu, Matthias Fey, Marinka Zitnik, Yuxiao Dong, Hongyu Ren, Bowen Liu, Michele Catasta, and Jure Leskovec. Open Graph Benchmark: Datasets for Machine Learning on Graphs, 2020. URL <https://arxiv.org/abs/2005.00687>. Version Number: 7.

Sergey Ioffe and Christian Szegedy. Batch Normalization: Accelerating Deep Network Training by Reducing Internal Covariate Shift, 2015. URL <https://arxiv.org/abs/1502.03167>. Version Number: 3.

Shaoxiong Ji, Shirui Pan, Erik Cambria, Pekka Marttinen, and Philip S. Yu. A Survey on Knowledge Graphs: Representation, Acquisition and Applications. *IEEE Transactions on Neural Networks and Learning Systems*, 33(2):494–514, February 2022. ISSN 2162-237X, 2162-2388. doi:10.1109/TNNLS.2021.3070843. URL <http://arxiv.org/abs/2002.00388>. arXiv: 2002.00388.

Rudolf Kadlec, Ondrej Bajgar, and Jan Kleindienst. Knowledge Base Completion: Baselines Strike Back, 2017. URL <https://arxiv.org/abs/1705.10744>. Version Number: 1.

Sekitoshi Kanai, Yasuhiro Fujiwara, Yuki Yamanaka, and Shuichi Adachi. Sigsoftmax: Reanalysis of the Softmax Bottleneck, 2018. URL <https://arxiv.org/abs/1805.10829>. Version Number: 1.

Seyed Mehran Kazemi and David Poole. SimpLE Embedding for Link Prediction in Knowledge Graphs, 2018. URL <https://arxiv.org/abs/1802.04868>. Version Number: 2.

Diederik P. Kingma and Jimmy Ba. Adam: A Method for Stochastic Optimization, 2014. URL <https://arxiv.org/abs/1412.6980>. Version Number: 9.

Timothée Lacroix, Nicolas Usunier, and Guillaume Obozinski. Canonical Tensor Decomposition for Knowledge Base Completion, 2018. URL <https://arxiv.org/abs/1806.07297>. Version Number: 1.

Yankai Lin, Zhiyuan Liu, Maosong Sun, Yang Liu, and Xuan Zhu. Learning Entity and Relation Embeddings for Knowledge Graph Completion. *Proceedings of the AAAI Conference on Artificial Intelligence*, 29(1), February 2015. ISSN 2374-3468, 2159-5399. doi:10.1609/aaai.v29i1.9491. URL <https://ojs.aaai.org/index.php/AAAI/article/view/9491>.

Yang Liu, Zequn Sun, Guangyao Li, and Wei Hu. I Know What You Do Not Know: Knowledge Graph Embedding via Co-distillation Learning, 2022. URL <https://arxiv.org/abs/2208.09828>. Version Number: 3.

Lorenzo Loconte, Nicola Di Mauro, Robert Peharz, and Antonio Vergari. How to Turn Your Knowledge Graph Embeddings into Generative Models, 2023. URL <https://arxiv.org/abs/2305.15944>. Version Number: 3.

Maximilian Nickel, Volker Tresp, and Hans-Peter Kriegel. A three-way model for collective learning on multi-relational data. In *Proceedings of the 28th International Conference on International Conference on Machine Learning*, ICML'11, pp. 809–816, Madison, WI, USA, June 2011. Omnipress. ISBN 978-1-4503-0619-5.

Maximilian Nickel, Kevin Murphy, Volker Tresp, and Evgeniy Gabrilovich. A Review of Relational Machine Learning for Knowledge Graphs. 2015. doi:10.48550/ARXIV.1503.00759. URL <https://arxiv.org/abs/1503.00759>. Publisher: arXiv Version Number: 3.

Aleksandar Pavlović and Emanuel Sallinger. ExpressivE: A Spatio-Functional Embedding For Knowledge Graph Completion, 2022. URL <https://arxiv.org/abs/2206.04192>. Version Number: 2.

Pouya Pezeshkpour, Yifan Tian, and Sameer Singh. Revisiting Evaluation of Knowledge Base Completion Models. February 2020. URL <https://openreview.net/forum?id=1uufzxsxfL>.

Daniel Ruffinelli, Samuel Broscheit, and Rainer Gemulla. You CAN Teach an Old Dog New Tricks! On Training Knowledge Graph Embeddings. April 2020. URL https://iclr.cc/virtual_2020/poster_BkxSmlBFvr.html.

Michael Schlichtkrull, Thomas N. Kipf, Peter Bloem, Rianne van den Berg, Ivan Titov, and Max Welling. Modeling Relational Data with Graph Convolutional Networks, 2017. URL <https://arxiv.org/abs/1703.06103>. Version Number: 4.

Warren D. Smith. D-dimensional orderings and Stirling numbers, 2014.

Nitish Srivastava, Geoffrey Hinton, Alex Krizhevsky, Ilya Sutskever, and Ruslan Salakhutdinov. Dropout: A Simple Way to Prevent Neural Networks from Overfitting. *Journal of Machine Learning Research*, 15(56):1929–1958, 2014. ISSN 1533-7928. URL <http://jmlr.org/papers/v15/srivastava14a.html>.

Danny Sullivan. A reintroduction to our Knowledge Graph and knowledge panels, May 2020. URL <https://blog.google/products/search/about-knowledge-graph-and-knowledge-panels/>.

Zhiqing Sun, Zhi-Hong Deng, Jian-Yun Nie, and Jian Tang. RotatE: Knowledge Graph Embedding by Relational Rotation in Complex Space, 2019. URL <https://arxiv.org/abs/1902.10197>. Version Number: 1.

Kristina Toutanova and Danqi Chen. Observed versus latent features for knowledge base and text inference. In *Proceedings of the 3rd Workshop on Continuous Vector Space Models and their Compositionality*, pp. 57–66, Beijing, China, 2015. Association for Computational Linguistics. doi:10.18653/v1/W15-4007. URL <http://aclweb.org/anthology/W15-4007>.

Théo Trouillon, Christopher R. Dance, Johannes Welbl, Sebastian Riedel, Éric Gaussier, and Guillaume Bouchard. Knowledge Graph Completion via Complex Tensor Factorization, 2017. URL <https://arxiv.org/abs/1702.06879>. Version Number: 2.

Shikhar Vashishth, Soumya Sanyal, Vikram Nitin, and Partha Talukdar. Composition-based Multi-Relational Graph Convolutional Networks, 2019. URL <https://arxiv.org/abs/1911.03082>. Version Number: 2.

Liang Wang, Wei Zhao, Zhuoyu Wei, and Jingming Liu. SimKGC: Simple Contrastive Knowledge Graph Completion with Pre-trained Language Models, 2022a. URL <https://arxiv.org/abs/2203.02167>. Version Number: 1.

Xintao Wang, Qianyu He, Jiaqing Liang, and Yanghua Xiao. Language Models as Knowledge Embeddings, 2022b. URL <https://arxiv.org/abs/2206.12617>. Version Number: 3.

Zhen Wang, Jianwen Zhang, Jianlin Feng, and Zheng Chen. Knowledge Graph Embedding by Translating on Hyperplanes. *Proceedings of the AAAI Conference on Artificial Intelligence*, 28(1), June 2014. ISSN 2374-3468, 2159-5399. doi:10.1609/aaai.v28i1.8870. URL <https://ojs.aaai.org/index.php/AAAI/article/view/8870>.

Bishan Yang, Wen-tau Yih, Xiaodong He, Jianfeng Gao, and Li Deng. Embedding Entities and Relations for Learning and Inference in Knowledge Bases, 2014. URL <https://arxiv.org/abs/1412.6575>. Version Number: 4.

Zhilin Yang, Zihang Dai, Ruslan Salakhutdinov, and William W. Cohen. Breaking the Softmax Bottleneck: A High-Rank RNN Language Model, 2017. URL <https://arxiv.org/abs/1711.03953>. Version Number: 4.

Zhilin Yang, Thang Luong, Ruslan Salakhutdinov, and Quoc Le. Mixtape: breaking the softmax bottleneck efficiently. In *Proceedings of the 33rd International Conference on Neural Information Processing Systems*, number 519, pp. 5775–5783. Curran Associates Inc., Red Hook, NY, USA, December 2019.

Zhaocheng Zhu, Zuobai Zhang, Louis-Pascal Xhonneux, and Jian Tang. Neural Bellman-Ford Networks: A General Graph Neural Network Framework for Link Prediction, 2021. URL <https://arxiv.org/abs/2106.06935>. Version Number: 4.

A TENSOR NOTATION

We borrow the notation from [Cichocki et al. \(2015\)](#) for tensors and matrices, summarized in Table 4.

Table 4: The tensor notation used throughout the paper.

Notation	Description
$\mathbf{A}, \mathbf{A}, \mathbf{a}, a$	tensor, matrix, vector, scalar
$\mathbf{A} = [\mathbf{a}_1 \dots \mathbf{a}_R]$	matrix \mathbf{A} with columns \mathbf{a}_r
$\mathbf{A} = \begin{bmatrix} \mathbf{a}_1 \\ \vdots \\ \mathbf{a}_R \end{bmatrix}$	matrix \mathbf{A} with rows \mathbf{a}_r
$a_{i_1, i_2, i_3, \dots, i_N}$	scalar of tensor \mathbf{A} obtained by fixing all indices
$\mathbf{a}_{\cdot, i_2, i_3, \dots, i_N}$	fiber of tensor \mathbf{A} obtained by fixing all but one index
$\mathbf{A}_{\cdot, \cdot, i_3, \dots, i_N}$	matrix slice of tensor \mathbf{A} obtained by fixing all but two indices
$\mathbf{A}_{\cdot, \cdot, \cdot, i_4, \dots, i_N}$	tensor slice of \mathbf{A} obtained by fixing some indices
$\mathbf{A}_{(n)} \in \mathbb{R}^{I_n \times I_1 I_2 \dots I_{n-1} I_{n+1} \dots I_N}$	mode- n unfolding of \mathbf{A}

B PROOFS

Proposition 3.1 (DR bottleneck). *A bottlenecked KGE constrained to a low-rank d cannot represent the distributions in a true adjacency matrix $\mathbf{Y} \in \{0, 1\}^{|\mathcal{E}||\mathcal{R}|\times|\mathcal{E}|}$ with rank $r > d + 1$ perfectly.*

Proof. Consider a perfect solution \mathbf{Z}^* for [DR](#) as introduced in [2.2](#), which assigns a uniform high score τ_+ to true triples and a uniform low score τ_- to false ones. The solution should satisfy $\mathbf{Y} = \frac{1}{\tau_+ - \tau_-}(\mathbf{Z}^* - \mathbf{1})$, where $\mathbf{1}$ is a matrix of ones with the same size as \mathbf{Y} . Since \mathbf{Z}^* has rank at most d and $\mathbf{1}$ is a matrix of rank at most 1, the equality is impossible if \mathbf{Y} has rank $r > d + 1$. \square

Theorem 3.2 (RR bottleneck). *A bottlenecked KGE with low-rank $d < |\mathcal{E}| - 1$ always has some unfeasible ranking configurations π , regardless of the learned input representations.*

Proof. We use a result from [Cover \(1967\)](#); [Good & Tideman \(1977\)](#); [Grivas et al. \(2022\)](#) which states that a linear (affine) classifier over N classes parameterised by a weight matrix $\mathbf{W} \in \mathbb{R}^{N \times d}$ (and bias vector $\mathbf{b} \in \mathbb{R}^N$) followed by any monotonic activation, can only predict a subset of class rankings if $d < N - 1$. Replacing $\mathbf{W} \in \mathbb{R}^{N \times d}$ with $\mathbf{E} \in \mathbb{R}^{|\mathcal{E}| \times d}$ yields the theorem. Additionally, for object vectors in general position, if we fix d , changing \mathbf{E} changes the set of rankings that are feasible, but not the cardinality of the set. The cardinality can be calculated using Stirling numbers with a proof that stems from finding the maximum and generic number of distance-based orderings of N points in a d -dimensional space ([Cover, 1967](#); [Good & Tideman, 1977](#); [Smith, 2014](#)). The narrower the low-rank d , the more class permutations π become infeasible. \square

Theorem 3.3 (SR bottleneck). *A bottlenecked KGE with low-rank $d < |\mathcal{E}|$ always has some unfeasible multi-label assignments configurations \mathbf{y} , regardless of the learned input representations.*

Proof. We use the result from [Cover \(1965\)](#); [Grivas et al. \(2023\)](#) which states that a linear (affine) classifier over N classes parameterised by a low-rank weight matrix $\mathbf{W} \in \mathbb{R}^{N \times d}$ (and bias vector $\mathbf{b} \in \mathbb{R}^N$) can only predict a subset of multi-label assignments configurations \mathbf{y} if $d < N$ using the decision rule $\text{sign}(\mathbf{W}\mathbf{x} + \mathbf{b})$ for input $\mathbf{x} \in \mathbb{R}^d$. Replacing $\mathbf{W} \in \mathbb{R}^{N \times d}$ with $\mathbf{E} \in \mathbb{R}^{|\mathcal{E}| \times d}$ yields the theorem. For a linear layer, the number of feasible assignments is upper-bounded by $2 \sum_{i=0}^{d-1} \binom{N-1}{i}$. For an affine layer, more assignments are feasible, but the increase in the number of feasible assignments is less than what would be achieved by increasing the embedding dimension d by one. \square

Theorem 4.1. *Let $\mathbf{Y} \in \{0, 1\}^{|\mathcal{E}||\mathcal{R}|\times|\mathcal{E}|}$ be the representation of the KG with subject-relation pairs on the first axis and objects on the second. Let the sign function $s(x) = 1$ if $x > 0$ and $s(x) = 0$ otherwise. Then, \mathbf{Y} can be exactly decomposed as $\mathbf{Y} = s(\mathbf{H}\mathbf{E}^\top)$ where $\mathbf{H} \in \mathbb{R}^{|\mathcal{E}||\mathcal{R}|\times(2c+1)}$,*

$\mathbf{E} \in \mathbb{R}^{|\mathcal{E}| \times (2c+1)}$, and c is the maximum out-degree across all subject-relation pairs in the KG. The function $s(\cdot)$ is applied element-wise.

Proof. We extend the approach of Chanpuriya et al. (2020); Alon et al. (1985) to the case of rectangular bipartite adjacency matrices $\mathbf{A} \in \{0, 1\}^{N \times M}$, where N represents the number of source nodes and M the number of destination nodes. c denotes the maximum out-degree of any source node. For the setting of Theorem 4.1, we take $N = |\mathcal{E}||\mathcal{R}|$ and $M = |\mathcal{E}|$.

Our goal is to decompose \mathbf{A} by expressing each row $\mathbf{a}_i \in \{0, 1\}^M$ through the equation

$$s(\mathbf{V}\mathbf{x}_i) = \mathbf{a}_i,$$

where

- $s(\cdot)$ is the sign function $s(z) = \begin{cases} 1, & \text{if } z > 0, \\ 0, & \text{if } z \leq 0, \end{cases}$
- $\mathbf{V} \in \mathbb{R}^{M \times (2c+1)}$ is a Vandermonde matrix – that is, a matrix with $2c + 1$ geometric progressions for M variables – with M rows associated to the destination nodes, and
- $\mathbf{x}_i \in \mathbb{R}^{2c+1}$ is a vector of polynomial coefficients associated with source node i .

That is, \mathbf{x}_i define the coefficients of a polynomial of degree $2c$ which, evaluated at each destination node $t = 1, \dots, M$, yields a score $p_i(t)$ that determines the sign of the edge between node i and node t .

If we successfully find such coefficients \mathbf{x}_i for each source node $i = 1, \dots, N$ – which will be guaranteed by the degree $2c$ of the polynomial –, then we can reconstruct the entire adjacency matrix \mathbf{A} as

$$\mathbf{A} = s(\mathbf{V}\mathbf{X}^\top),$$

where $\mathbf{X} \in \mathbb{R}^{N \times (2c+1)}$ is the matrix of coefficients \mathbf{x}_i for all source nodes stacked as rows.

Constructing the Vandermonde Matrix We define the Vandermonde matrix \mathbf{V} such that

$$v_{t,j} = t^{j-1}, \quad t = 1, \dots, M, \quad j = 1, \dots, 2c + 1.$$

That is, evaluating $\mathbf{V}\mathbf{x}_i \in \mathbb{R}^M$ means evaluating the $2c$ -degree polynomial $p_i(t)$ at the integers $t = 1, \dots, M$, each integer t representing a destination node.

Fitting the Polynomials Next, we wish to construct the coefficients \mathbf{x}_i such that the polynomial $p_i(t)$ matches the adjacency pattern \mathbf{a}_i :

- $p_i(t) > 0$ for indices where $a_{i,t} = 1$ and
- $p_i(t) < 0$ for indices where $a_{i,t} = 0$.

To achieve this, we choose $p_i(t)$ to have roots at appropriate locations in the intervals between the integer points.

Consider for example the adjacency pattern $\mathbf{a}_i = [0 \ 0 \ 1 \ 0 \ 1 \ 0]$. We need $p_i(t)$ to be positive for $t = 3$ and $t = 5$ and negative for all other t . We can choose $p_i(t)$ to have two roots at $t = 3 \pm \epsilon$ and two roots at $t = 5 \pm \epsilon$, where $0 < \epsilon < 1$, and ensuring that the polynomial has positive signs where needed. This is illustrated in Figure 4a.

In general, if the polynomial has degree $2c$, we can always find $2c$ roots that isolate the (at most c) points where $p_i(t)$ is positive. As a side note, notice that this degree requirement is an upper bound. *In practice, the bound can be made tighter depending on the ordering of the entities in the adjacency matrix.* In some cases, the ones in \mathbf{a}_i may appear consecutively (forming *blocks*) so that fewer sign changes are needed. This is particularly likely for graphs with high clustering coefficients, in which case each cluster can be grouped in the ordering (Figure 4b). Finding the optimal ordering is a hard problem and is dataset-specific. Intuitively, datasets that follow power-law degree distributions should

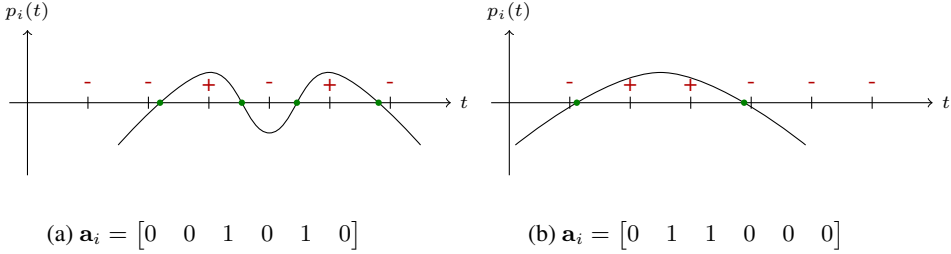


Figure 4: Fitting a polynomial $p_i(t)$ to the adjacency pattern \mathbf{a}_i . The sign of $p_i(t)$ at each integer $t = 1, \dots, M$ indicates the existence of an edge from i to t . **(a) For any adjacency pattern with c connections, there exists a polynomial of degree $2c$ that represents the pattern.** This polynomial has $2c$ roots, shown as green dots, which isolate the c points where $p_i(t)$ is positive. **(b) With a better ordering of the ones in \mathbf{a}_i , the polynomial may require a lower degree.** Fewer sign changes are needed if the ones in \mathbf{a}_i form blocks.

be easier to fit, because the ordering needs to be optimised only for the few entities that have many connections. *This is why the average out-degree also gives an important hint on the difficulty of the dataset.*

Reconstructing the Adjacency Matrix Once we have determined a coefficient vector \mathbf{x}_i for each source node i , we construct the matrix $\mathbf{X} \in \mathbb{R}^{N \times (2c+1)}$ by stacking them as rows. Then, the entire adjacency matrix can be written as $\mathbf{A} = s(\mathbf{V}\mathbf{X}^\top)$, yielding the desired result.

Interpreting the Embeddings This decomposition suggests a natural interpretation in terms of node embeddings. Each destination node t corresponds to an object o and is embedded as the vector

$$\mathbf{v}_t = [1 \ t \ t^2 \ \dots \ t^{2c}],$$

corresponding to evaluating the polynomial basis at t . Each source node i corresponds to a subject-relation pair (s, r) and is embedded as the coefficient vector \mathbf{x}_i defining the polynomial $p_i(t)$. The dot product $\mathbf{v}_t^\top \mathbf{x}_i = p_i(t)$ determines the sign at (i, t) , i.e., the existence of the triple (s, r, o) . \square

C SUBJECT PREDICTION

Subject prediction is the task of predicting suitable subject entities for $(?, r, o)$ queries. There are conventionally two main approaches to subject prediction with KGE models.

Vector-matrix multiplication Bilinear models (see Section 2.1) can be used to score all subject entities against a relation-object pair as a vector-matrix multiplication:

$$\mathbf{z}_{?,r,o} = \mathbf{E}\mathbf{h}_{r,o} \quad (4)$$

where $\mathbf{h}_{r,o} \in \mathbb{R}^d$ is an embedded representation of the relation-object pair (r, o) and $\mathbf{E} \in \mathbb{R}^{|\mathcal{E}| \times d}$ is the embedding matrix of all subject entity candidates. For example, in RESCAL’s score function $\mathbf{e}_s^\top \mathbf{W}_r \mathbf{e}_o$ Nickel et al. (2011), we have $\mathbf{h}_{r,o} = \mathbf{W}_r \mathbf{e}_o$, where $\mathbf{W}_r \in \mathbb{R}^{d \times d}$ is a matrix of shared parameters for relation r . In the score function $(\mathbf{e}_s \odot \mathbf{w}_r)^\top \mathbf{e}_o$ of DISTMULT (Yang et al., 2014), we have $\mathbf{h}_{r,o} = \mathbf{w}_r \odot \mathbf{e}_o$, where \odot is the element-wise (Hadamard) product, and $\mathbf{e}_s, \mathbf{w}_r, \mathbf{e}_o \in \mathbb{R}^d$. Under this perspective, our theoretical results on rank bottlenecks in KGEs for solving object prediction (Section 3) can be extended to subject prediction by replacing the hidden state $\mathbf{h}_{s,r}$ with $\mathbf{h}_{r,o}$. But, our KGE-MoS solution is not applicable simultaneously for both object and subject prediction as the mixture of softmaxes breaks the bilinearity of the score function.

Inverse relations The most general approach which applies to all KGE methods – including neural network methods – is to introduce inverse relations r^{-1} and to convert the subject prediction query $(?, r, o)$ into an object prediction query $(o, r^{-1}, ?)$ (Dettmers et al., 2017; Lacroix et al., 2018). This

introduces $|\mathcal{R}|$ new relations and embeddings, but this parameter count is often negligible compared to the number of parameters of the entities.

$$\mathbf{z}_{:,r,o} := \mathbf{z}_{o,r^{-1},:} = \mathbf{h}_{o,r^{-1}} \mathbf{E}^\top \quad (5)$$

In this case, both the theoretical results and the KGE-MoS solution are immediately applicable. We can use the same KGE-MoS layer as follows:

$$P(S|o, r^{-1}) = \sum_{k=1}^K \pi_{o,r^{-1},k} \text{softmax}(f_k(\mathbf{h}_{o,r^{-1}}) \mathbf{E}^\top), \quad \sum_{k=1}^K \pi_{o,r^{-1},k} = 1 \quad (6)$$

where S is a random variable that ranges over the same entities as O .

D BACKGROUND (CONT.)

D.1 OBJECT PREDICTION AS A VECTOR-MATRIX MULTIPLICATION

In this section, we elaborate on how to rewrite the different KGE models as a function linear in the object embedding $\phi(s, r, o) = \mathbf{h}_{s,r}^\top \mathbf{e}_o$, with $\mathbf{h}_{s,r}, \mathbf{e}_o \in \mathbb{R}^d$.

Bilinear models In RESCAL’s score function $\mathbf{e}_s^\top \mathbf{W}_r \mathbf{e}_o$ Nickel et al. (2011), we have $\mathbf{h}_{s,r}^\top = \mathbf{e}_s^\top \mathbf{W}_r$, where $\mathbf{W}_r \in \mathbb{R}^{d \times d}$ is a matrix of shared parameters for relation r . In the score function $(\mathbf{e}_s \odot \mathbf{w}_r)^\top \mathbf{e}_o$ of DISTMULT (Yang et al., 2014), we have $\mathbf{h}_{s,r}^\top = (\mathbf{e}_s \odot \mathbf{w}_r)^\top$, where \odot is the element-wise (Hadamard) product, and $\mathbf{e}_s, \mathbf{w}_r, \mathbf{e}_o \in \mathbb{R}^d$. The same can be derived for COMPLEX (Trouillon et al., 2017), an extension of DISTMULT to complex-valued embeddings to handle asymmetry in the score function, or for CP (Lacroix et al., 2018) and SIMPLE (Kazemi & Poole, 2018), which use different embedding spaces for subjects and objects – though COMPLEX and SIMPLE with embedding sizes d give forms $\mathbf{h}_{s,r}^\top \mathbf{e}_o$ with bottleneck dimension $2d$ as we detail in the next paragraph. Finally, TUCKER (Balažević et al., 2019) decomposes the score tensor $\mathcal{Z} \in \mathbb{R}^{|\mathcal{E}| \times |\mathcal{R}| \times |\mathcal{E}|}$ as $\mathcal{Z} = \mathbf{W} \times_1 \mathbf{E} \times_2 \mathbf{R} \times_3 \mathbf{E}$ where $\mathbf{W} \in \mathbb{R}^{d \times d_r \times d}$ is a core tensor of shared parameters across all entities and relations and \times_n are mode- n products.³ $\mathbf{E} \in \mathbb{R}^{|\mathcal{E}| \times d}$, $\mathbf{R} \in \mathbb{R}^{|\mathcal{R}| \times d_r}$ are entity and relation embeddings, respectively. The score function is then $\phi_{\text{TUCKER}}(s, r, o) = \mathbf{W} \times_1 \mathbf{e}_s \times_2 \mathbf{w}_r \times_3 \mathbf{e}_o$. Let $\mathbf{h}_{s,r} = \mathbf{W} \times_1 \mathbf{e}_s \times_2 \mathbf{w}_r \in \mathbb{R}^d$. Then, $\phi_{\text{TUCKER}}(s, r, o) = (\mathbf{h}_{s,r}^{\text{TUCKER}})^\top \mathbf{e}_o$. Specific implementations of the core tensor \mathbf{W} recovers the other bilinear models as special cases.

COMPLEX, SIMPLE As explained by Kazemi & Poole (2018); Balažević et al. (2019), COMPLEX (Trouillon et al., 2017) can be seen as a special case of TUCKER and bilinear models by considering the real and imaginary part of the embedding concatenated in a single vector, e.g., $[\text{Re}(\mathbf{e}_o); \text{Im}(\mathbf{e}_o)] \in \mathbb{R}^{2d}$ for the object. We detail this to highlight that the rank bottleneck for these models is $2d$ rather than d . The score function of COMPLEX is

$$\begin{aligned} \phi_{\text{COMPLEX}}(s, r, o) = & (\text{Re}(\mathbf{e}_s) \odot \text{Re}(\mathbf{w}_r))^\top \text{Re}(\mathbf{e}_o) + (\text{Im}(\mathbf{e}_s) \odot \text{Re}(\mathbf{w}_r))^\top \text{Im}(\mathbf{e}_o) \\ & (\text{Re}(\mathbf{e}_s) \odot \text{Im}(\mathbf{w}_r))^\top \text{Im}(\mathbf{e}_o) - (\text{Im}(\mathbf{e}_s) \odot \text{Im}(\mathbf{w}_r))^\top \text{Re}(\mathbf{e}_o) \end{aligned}$$

Let us define $\mathbf{h}_{sr}^1 = \text{Re}(\mathbf{e}_s) \odot \text{Re}(\mathbf{w}_r) - \text{Im}(\mathbf{e}_s) \odot \text{Im}(\mathbf{w}_r)$ and $\mathbf{h}_{sr}^2 = \text{Im}(\mathbf{e}_s) \odot \text{Re}(\mathbf{w}_r) + \text{Re}(\mathbf{e}_s) \odot \text{Im}(\mathbf{w}_r)$, with $\mathbf{h}_{sr}^1, \mathbf{h}_{sr}^2 \in \mathbb{R}^d$. We have

$$\phi_{\text{COMPLEX}}(s, r, o) = (\mathbf{h}_{sr}^1)^\top \text{Re}(\mathbf{e}_o) + (\mathbf{h}_{sr}^2)^\top \text{Im}(\mathbf{e}_o).$$

Concatenating the real and imaginary parts of \mathbf{e}_o into a single vector $\mathbf{e}_o^{\text{COMPLEX}} = [\text{Re}(\mathbf{e}_o); \text{Im}(\mathbf{e}_o)] \in \mathbb{R}^{2d}$, and concatenating the hidden vectors \mathbf{h}_{sr}^1 and \mathbf{h}_{sr}^2 into a single vector $\mathbf{h}_{sr}^{\text{COMPLEX}} = [\mathbf{h}_{sr}^1; \mathbf{h}_{sr}^2] \in \mathbb{R}^{2d}$, we have

$$\phi_{\text{COMPLEX}}(s, r, o) = (\mathbf{h}_{sr}^{\text{COMPLEX}})^\top \mathbf{e}_o^{\text{COMPLEX}}$$

which is linear in the object embedding $\mathbf{e}_o^{\text{COMPLEX}}$, this time with bottleneck dimension $2d$. A similar trivial result can be done for SIMPLE Kazemi & Poole (2018), again considering the concatenation of two embeddings in a single vector in \mathbb{R}^{2d} .

³The mode- n product $\mathbf{X} \times_n \mathbf{A}$ is the tensor obtained by multiplying each slice of \mathbf{X} along the n -th mode by the corresponding column of \mathbf{A} . That is, $(\mathbf{X} \times_n \mathbf{A})_{i_1 \dots i_{n-1} j i_{n+1} \dots i_N} = \mathbf{a}_{j,:}^\top \mathbf{x}_{i_1, \dots, i_{n-1}, i_{n+1}, \dots, i_N}$.

Neural KGEs CONVE (Dettmers et al., 2017) scores triples as $f(\text{vec}(f([\mathbf{e}_s; \mathbf{w}_r] * \mathbf{w})) \mathbf{W})^\top \mathbf{e}_o$, with f a non-linearity, $*$ a convolution operator, and vec a vectorization operator. The score function is linear in the object embedding \mathbf{e}_o . Similarly, STARE (Galkin et al., 2020) uses a score function $\text{Linear}(\text{SumPooling}(\text{Transformer}([\mathbf{e}_s + \text{pe}[0]; \mathbf{w}_r + \text{pe}[1]])))^\top \mathbf{e}_o$, where pe are positional encodings, that has non-linearities in the transformer and pooling constructing $\mathbf{h}_{s,r}$ but that is still linear in the object embedding \mathbf{e}_o . R-GCNs (Schlichtkrull et al., 2017) and COMPGCN (Vashishth et al., 2019) use powerful message passing schemes to build node representations for the entities \mathbf{e}_s and \mathbf{e}_o , but still use a simple bilinear scoring function to score triples given the resulting representations – DISTMULT’s score function giving the best performance. Language-based models like SIMKGC (Wang et al., 2022a) or MEMKGC (Choi et al., 2021) use BERT or other masked language models to encode powerful entity and relation embeddings \mathbf{e}_s , \mathbf{e}_o and \mathbf{w}_r , but still use a linear projection to score objects in their final layer. COLE (Liu et al., 2022) uses two heads, one transformer and one BERT, and both use a linear output layer to score objects. LMKE (Wang et al., 2022b) is designed for triple classification but has a variant C-LMKE designed for link prediction, which uses a linear output layer where rows correspond to entities embeddings \mathbf{e}_o .

D.2 OUTPUT FUNCTIONS IN KGEs

In this section, we further detail the different output functions that KGEs parameterized over the years and the loss functions that were used to train them.

Raw scores with margin-based loss (RR) Early KGEs (Bordes et al., 2013; Yang et al., 2014) used margin-based loss functions for ranking reconstruction (RR). The loss ensures that the scores of true triples are higher than the scores of false triples by at least a margin $\gamma > 0$, but does not ensure sign or calibrated reconstruction.

Sigmoid layers with BCE loss (RR, SR, possibly DR) Trouillon et al. (2017), followed by Dettmers et al. (2017), proposed to use binary cross-entropy (BCE) loss between the scores and the binary representation of the graph. They define a sigmoid layer $P(y_o = 1 | \mathbf{h}_{s,r}) = \sigma(\mathbf{h}_{s,r}^\top \mathbf{e}_o)$, where $y_o = 1$ if $(s, r, o) \in \mathcal{G}$ and 0 otherwise. This defines a multi-label classifier with predictions $\hat{\mathbf{y}} = \mathbb{1}(\mathbf{E}\mathbf{h}_{s,r} > 0) \in \{0, 1\}^{|\mathcal{E}|}$ where $\mathbb{1}$ is the indicator function applied element-wise and the i -th entry is the binary prediction for object i . This classifier naturally aligns with sign-label reconstruction (SR). Calibrated scores (DR) were not a concern in this setting until Arakelyan et al. (2021; 2023) started to combine the binary prediction scores of several simple queries to answer complex queries, which requires the scores to be calibrated.

Softmax layers with CE loss (RR, possibly DR) Kadlec et al. (2017) proposed to use a cross-entropy (CE) loss. For a query $(s, r, ?)$, they define a vector of probabilities $\mathbf{p}_{s,r} = \text{softmax}(\mathbf{E}\mathbf{h}_{s,r}) \in \Delta^{|\mathcal{E}|}$, with $\Delta^{|\mathcal{E}|}$ the probability simplex over the objects. Here, softmax is applied element-wise to get the components $p_{s,r,o} = \exp(\mathbf{h}_{s,r}^\top \mathbf{e}_o) / \sum_{o' \in \mathcal{E}} \exp(\mathbf{h}_{s,r}^\top \mathbf{e}_{o'})$. This vector should align with the data distribution (labels of the corresponding triples, normalized to sum to 1). Although softmax is typically used for predicting a single correct class, here it is repurposed for multi-label scenarios by retrieving top- k entries and ranking likely completions (RR). This modeling also opens the door to sampling (Loconte et al., 2023) which requires calibrated scores (DR).

In comprehensive benchmarking efforts, Ruffinelli et al. (2020) and Ali et al. (2022) re-evaluated all score functions with all possible output functions and loss functions for ranking reconstruction (RR). They found that softmax-based modeling generally outperform other approaches, closely followed by modeling with BCE loss. Models trained with margin-based loss functions were consistently the worst performing. Note that the authors did not evaluate the performance of models for sign-label reconstruction (SR) or calibrated score reconstruction (DR).

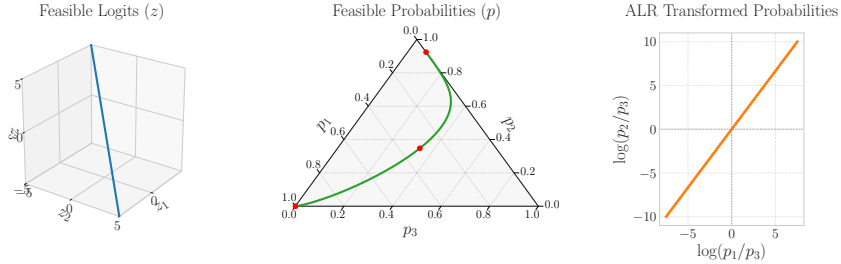


Figure 5: Visualisation of the softmax bottleneck. The **blue** line is the linear subspace of feasible scores for a fixed matrix \mathbf{E} , where each point is calculated for a different hidden state $\mathbf{h}_{s,r}$. The **green** line is the set of feasible probability distributions after the softmax function. The **orange** line is the additive-log ratio of the probabilities. **The feasible distributions are constrained to a manifold that is linear in the ALR space.** Any groundtruth that does not respect this constraint cannot be represented by the model.

E RANK BOTTLENECKS IN KGES (CONT.)

E.1 LOG-LINEARITY OF THE SOFTMAX BOTTLENECK

As we mention in 3.1, the softmax function maps the d -dimensional linear subspace of scores to a smooth d -dimensional manifold within the $(|\mathcal{E}|-1)$ -dimensional probability simplex $\Delta^{|\mathcal{E}|}$. While this manifold is non-linear, its shape is relatively simple and can be described by the following constraint: its composition with the log function is a linear function of the scores. An algebraic perspective on this bottleneck is provided by Yang et al. (2017). Let $\mathbf{A} \in \mathbb{R}^{|\mathcal{E}||\mathcal{R}| \times |\mathcal{E}|}$ be the log-probability matrix where $a_{i,j} = \log P(O=j|\mathbf{h}_i)$. We have

$$\mathbf{A} = \begin{bmatrix} \log \text{softmax}(\mathbf{E}\mathbf{h}_{1,1}) \\ \vdots \\ \log \text{softmax}(\mathbf{E}\mathbf{h}_{|\mathcal{E}|,|\mathcal{R}|}) \end{bmatrix} = \mathbf{H}\mathbf{E}^\top - \begin{bmatrix} c_{1,1} \\ \vdots \\ c_{|\mathcal{E}|,|\mathcal{R}|} \end{bmatrix} [1 \quad \cdots \quad 1]$$

where $c_i = \log \sum_{j=1}^{|\mathcal{E}|} \exp(\mathbf{E}\mathbf{h}_i)_j \in \mathbb{R}$ is the log-partition function. Since $\mathbf{H}\mathbf{E}^\top$ has a rank at most d , and the term involving log-partition functions has a rank at most 1, the resulting log-probability matrix \mathbf{A} has a rank of at most $d+1$.

We can visualise this log-linearity using log-ratio transformations. For example, for a vector of probabilities $\mathbf{p} \in \Delta^{|\mathcal{E}|}$, we use an Additive Log-Ratio (ALR) transformation with $p_{|\mathcal{E}|}$ as the reference:

$$\text{ALR}(\mathbf{p}) = \begin{bmatrix} \log \frac{p_1}{p_{|\mathcal{E}|}} \\ \vdots \\ \log \frac{p_{|\mathcal{E}|-1}}{p_{|\mathcal{E}|}} \end{bmatrix} \quad (7)$$

This transformation maps the simplex to a $d-1$ dimensional space where the log-partitions are eliminated in the ratios. As we visualise in Figure 5, the log-ratio of the probabilities span a linear subspace of the possible probability ratios. Any groundtruth that does not respect this log-linear constraint cannot be represented by the model.

F EXPERIMENTS

F.1 DATASETS

We use the usual splits for FB15K237 Toutanova & Chen (2015), WN18RR Dettmers et al. (2017) and ogbl-biokg Hu et al. (2020). openbiolink Breit et al. (2020) comes with four available datasets. We use the high-quality, directed set downloadable from the PyKeen library Ali et al. (2020), which filters out test entities that do not appear in the training set and are not learnable by knowledge

graph embedding models. Hetionet [Himmelstein et al. \(2017\)](#) does not come with pre-defined splits. We obtain the splits via the PyKeen library using a seed of 42. Table 5 reports statistics for all datasets.

Table 5: Dataset statistics and (s, r, \cdot) out-degrees. The sufficient bound d_{SR}^+ for exact sign reconstruction is calculated based on the maximum out-degree according to Theorem 4.1.

Dataset	#Entities	#Rels	#Triples	Inverse Relations	Out-Degree			d_{SR}^+
					Mean	Median	Max	
FB15k-237	14,541	237	310,116	✗	3.03	1	954	1,909
				✓	3.83	1	4,364	8,729
WN18RR	40,943	11	93,003	✗	1.40	1	473	947
				✓	1.70	1	510	1,021
Hetonet	45,158	24	2,250,197	✗	29.07	7	15,036	30,073
				✓	21.66	6	15,036	30,073
ogbl-biokg	93,773	51	5,088,434	✗	40.54	14	29,328	58,657
				✓	37.48	12	29,328	58,657
openbiolink	180,992	28	4,559,267	✗	14.47	2	2,251	4,503
				✓	18.12	2	18,420	36,841

F.2 METRICS

Filtered NLL The negative log-likelihood (NLL) metric measures how well a model assigns probability to the true triples in the test set. However, in KGC, because the training and test sets are disjoint, a model trained to assign high probability to training triples might leave little probability mass for test triples, even if they follow similar patterns. In this case, the NLL can unfairly penalise models that fit the training set well but are able to generalise out-of-distribution, as generalisation in KGC is always *out-of-distribution* rather than in-distribution.

To address this issue, we use a filtered version of NLL when evaluating on the test set. For a $(s, r, ?)$ query, we zero out the probabilities of ground truth objects for that query seen during training, renormalising the probabilities of the model predictions. Formally, given a model prediction $P(o|s, r)$, we define the filtered test probability as

$$P^{\text{filtered}}(o|s, r) = \frac{\mathbb{1}[(s, r, o) \notin \mathcal{G}_{\text{train}}]P(o|s, r)}{\sum_{o' \in \mathcal{E}} \mathbb{1}[(s, r, o') \notin \mathcal{G}_{\text{train}}]P(o'|s, r)} \quad (8)$$

This filtered approach provides a more meaningful evaluation of the model’s ability to generalize to unseen triples, as it focuses on the model’s ability to distinguish test triples from truly negative samples rather than from training triples that the model has already learned. It prevents situations where a model that accurately assigns high probability to training instances might be unfairly disadvantaged compared to a less informed model when evaluating predictions on the disjoint test set (Figure 6).

Ranking metrics The quality of a KGC model is commonly assessed by ranking the scores of test triples $(s, r, o) \in \mathcal{G}_{\text{test}}$. For example, in the context of object prediction, the ranks are computed as

$$R_{\theta}(s, r, o) := 1 + \sum_{e \in \mathcal{E}'} \mathbb{I}[\Phi_{\theta}(s, r, e) > \Phi_{\theta}(s, r, o)]. \quad (9)$$

where $\mathbb{I}[\cdot]$ is the indicator function and the set $\mathcal{E}' := \{e \in \mathcal{E} \mid (s, r, e) \notin \mathcal{G}\}$ filters the rank by only including object entities that do not form KG triples. A pessimistic version of the rank is sometimes considered by taking a non-strict inequality. The mean reciprocal rank (MRR) is the mean of the reciprocal ranks $\text{MRR} = \frac{1}{|\mathcal{G}_{\text{test}}|} \sum_{(s, r, o) \in \mathcal{G}_{\text{test}}} R_{\theta}(s, r, o)^{-1}$. The mean rank (MR) is the arithmetic mean of the ranks, but is notably sensitive to outliers. The Hits@k metric is the proportion of test triples that are ranked within the top k positions.

Notice that in `ogbl-biokg`, each test object for $(s, r, ?)$ are not ranked against all entities, but only against a pre-defined set of 500 entities. The same holds for subject prediction $(?, r, o)$.

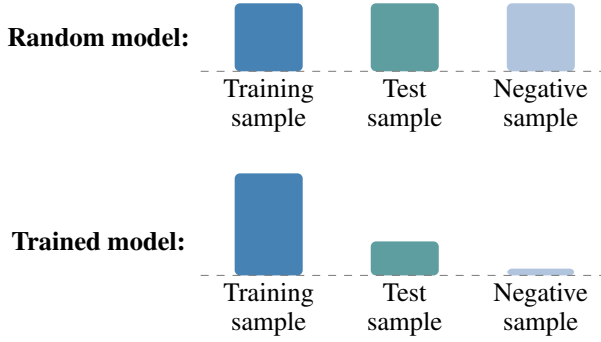


Figure 6: Likelihood assigned by models to training/test/random samples (conceptual graph). Because in KGC the set of training and test samples are disjoint, trained models leave less probability mass for test samples even if the model would assign higher probability to test samples if training samples were not options.

F.3 EXPERIMENTAL SETTING

General Hyperparameters We guide the choice of hyperparameters by guidelines from the original papers of each model, as well as insights from recent benchmarking papers Ruffinelli et al. (2020); Ali et al. (2022). All baseline models are trained using the Adam optimizer Kingma & Ba (2014) with a learning rate of 10^{-4} , except for DISTMULT and COMPLEX (without KGE-MoS), which use a higher learning rate of 10^{-3} due to their shallow architecture. We use a batch size of 1000 for all models as KGEs are more stable with larger batch sizes Ruffinelli et al. (2020), except for RESCAL, RESCAL-MoS, COMPGCN and COMPGCN-MoS, which use a batch size of 500 on `ogbl-biokg` and `openbiolink` for memory constraints. The models are trained for 30 training set epochs, with early stopping according to validation set metrics at a patience of 8 epochs.

Regularisation Following the findings of Ruffinelli et al. (2020), which showed that dropout Srivastava et al. (2014) is more effective than norm-based regularisation for KGEs, we apply a dropout of 0.1 to the encoded representation $\mathbf{h}_{s,r}$ (recalling that models can be represented as $\phi(s, r, o) = \mathbf{h}_{s,r}^\top \mathbf{e}_o$). An exception to this is CONVE, which already incorporates dropout within its neural network layers.

CONVE specific hyperparameters For CONVE, we adopt the hyperparameter settings from its original paper Dettmers et al. (2017). The model reshapes the input subject and relation embeddings into two-dimensional "images" (height 8), followed by a two-layer convolutional network with 32 channels and a kernel size of (3, 3). The output is then passed through a fully connected layer to obtain $\mathbf{h}_{s,r}$. Regularisation for CONVE includes dropout on embeddings (0.2), feature maps after convolution (0.3), and the output of the fully connected layer (0.3). Each layer in CONVE is also followed by a batch normalisation layer Ioffe & Szegedy (2015).

COMPGCN specific hyperparameters For COMPGCN, we use the following hyperparameters: initial embedding dimension of 100 for entities and relations and GCN dimension (which dictates the bottleneck) of $d = 200$, $d = 100$ or $d = 50$ depending on the dataset. We use a single GCN layer without bias terms and use COMPGCN without basis decomposition. Dropout is applied at two stages: 0.1 dropout in the GCN layer and 0.1 hidden dropout after the GCN layer. For the composition operation in COMPGCN, we use DISTMULT as was empirically shown to be the best option in the original paper Vashisht et al. (2019).

KGE-MoS details and hyperparameters For the KGE-MoS layer, defined as:

$$P(O|s, r) = \sum_{k=1}^K \pi_{s,r,k} \text{softmax}(f_k(\mathbf{h}_{s,r}) \mathbf{E}^\top), \quad \sum_{k=1}^K \pi_{s,r,k} = 1 \quad (10)$$

we use two-layer projections for $f_k(\mathbf{h}_{s,r})$, maintaining the same intermediate dimension d as the KGE dimension. Each projection layer is followed by batch normalisation Ioffe & Szegedy (2015),

Table 6: Empirical rank of the log-probability matrix for DISTMULT-MoS on the test set of FB15k-237.

Model	Empirical rank
DISTMULT-MoS, $K = 1, d = 200$	201
DISTMULT-MoS, $K = 4, d = 200$	3,651
DISTMULT-MoS, $K = 1, d = 1000$	1,001
DISTMULT-MoS, $K = 4, d = 1000$	14,541

a non-linear activation, and hidden dropout (applied in that order). To encourage the use of all mixture components, we incorporate the entropy of the distribution defined by the mixture weights $(\pi_{s,r,1}, \dots, \pi_{s,r,K})$ into the loss function. Our hyperparameter search for KGE-MoS involved a random exploration over learning rate (10^{-2} to 10^{-5} , log-scale), hidden dropout (0.0 to 0.2), activation type (ReLU, LeakyReLU, GeLU, tanh), and entropy regularisation weight (10^{-7} to 1.0, log-scale). The final reported results for KGE-MoS were obtained with a learning rate of 10^{-4} , hidden dropout of 0.1, LeakyReLU activation, and an entropy regularisation weight of 10^{-3} .

Parameters initialisation Parameters for the KGEs and all model layers are initialised using Xavier uniform initialisation [Glorot & Bengio \(2010\)](#). Repeated runs are performed with different initialisation seeds for statistical significance.

Hardware All experiments are run on NVIDIA A10 GPUs with 24GB of memory. Time of execution for each baseline ranges from a couple of hours for FB15K237, the smallest dataset, to 1-2 days for openbiolink, the largest dataset.

F.4 ADDITIONAL RESULTS

F.4.1 STANDARD DEVIATIONS AND HITS@ METRICS

Tables 9, 10, 11, 12 and 13 report the full results for the FB15k-237, Hetionet, ogbl-biokg, openbiolink, and WN18RR datasets, respectively.

Note that results for COMPLEX use halved embedding sizes $d = 100$ and $d = 500$ because it has real and imaginary parts leading to a rank bottleneck of $2d$ (see Appendix D.1).

On the other hand, while results for COMPGCN use $d = 200$ on FB15k-237 and Hetionet and are comparable to the other models, they are conducted with $d = 100$ on ogbl-biokg, and $d = 50$ on openbiolink due to computational constraints.

F.4.2 EMPIRICAL RANK

Borrowing the idea of [Yang et al. \(2017\)](#), we confirm empirically that KGE-MoS breaks the rank bottleneck by measuring the rank of the log-probability matrix measured on the test data for $K = 1$ softmax and $K > 1$ softmaxes. That is, we compute the rank of

$$\begin{bmatrix} \log P(O|sr_1) \\ \vdots \\ \log P(O|sr_{N_{\text{test}}}) \end{bmatrix}$$

where sr_i ranges over subject relation pairs in the test set.

We find the empirical ranks in Table 6. When $K = 1$, the rank is as expected $d + 1$ (where d is the rank of the logits and 1 is the rank of the log partition matrix). **Increasing K quickly increases the empirical rank.** In fact, as in FB15k-237, the number of entities $|\mathcal{E}| = 14,951$, the matrix is even **full rank** when $d = 1000$ and $K > 1$. In other words, the bottleneck is effectively broken.

F.4.3 INFERENCE TIME

In Table 7 we report inference time results for all methods.

Table 7: Inference and backpropagation time for a single minibatch on `openbiolink` at $d = 1000$. RESCAL and RESCAL-MoS are compared at batch size 500 to fit on device memory. Other models are compared at batch size 1000.

Model	Time per batch (ms)
DISTMULT	1.34
DISTMULT-MoS ($K = 1$)	3.30
DISTMULT-MoS ($K = 4$)	3.69
RESCAL	1.51
RESCAL-MoS ($K = 1$)	3.49
RESCAL-MoS ($K = 4$)	3.42
CONVE	2.72
CONVE-MoS ($K = 1$)	4.74
CONVE-MoS ($K = 4$)	4.60

Table 8: Results on `ogbl-biokg` at $d = 5000$. Breaking rank bottlenecks does not improve performance when the dimension is sufficiently large. However, increasing d comes at the cost of sacrificing critical hyperparameters such as batch size due to GPU memory constraints which deteriorates performance.

Model ($d = 5000$)	NLL	MRR	Param
DISTMULT-MoS, $K = 1$	4.54	0.79	519.4M
DISTMULT-MoS, $K = 4$	4.54	0.79	669.5M

F.4.4 BOTTLENECKS IN HIGHER-DIMENSIONAL SETTINGS ON OGBL-BIOKG

Next, we target a negative result: we evaluate whether KGE-MoS still shows a significant performance gain when the embedding dimension d is sufficiently large. Indeed, for a sufficiently large dimension d (dataset dependent), the bottleneck impact is not as great. Our results on `FB15K-237` and `WN18RR` (small datasets) aim to demonstrate this. We try to replicate this insight on one of the larger datasets (`ogbl-biokg`, the most densely connected one) with $d = 5000$.

We had to reduce our batch size from 1000 to 200 samples to accommodate for the larger dimension in the GPU memory (24GB). We measure two baselines, (i) DISTMULT-MoS with $K = 1$, (ii) DISTMULT-MoS with $K = 4$. DISTMULT-MoS with $K = 1$ does not break the rank bottleneck, but is included to isolate the effect of adding an asymmetric layer to DISTMULT vs breaking the rank bottleneck (see our paragraph "Mixture Ablation" in Section 6.1).

The results gives us two findings. (i) Breaking the rank bottleneck does not notably improve the performance on `ogbl-biokg` when $d = 5000$ (DISTMULT-MoS, $K = 4 \approx$ DISTMULT-MoS, $K = 1$). (ii) However, lowering the batch size to fit the model at $d = 5000$ in memory strongly deteriorates the performance compared to the baselines at $d = 1000$ (compare these results with those of Table 11). In other words, **the simple solution of increasing the embedding dimension, in addition to using vastly more parameters, comes at the cost of sacrificing critical hyperparameters such as batch size which deteriorates performance**.

Table 9: Full results for the FB15k-237 dataset.

Model	FB15k-237						
	NLL↓	MRR↑	MR↓	Hits@1↑	Hits@3↑	Hits@10↑	Param
<i>d</i> = 200							
DISTMULT	4.74±.08	.304±.004	228±7.5	.216±.003	.331±.005	.482±.004	3.0M
DISTMULT-MOS	4.65±.01	.306±.002	214±0.3	.220±.002	.336±.001	.479±.003	3.3M
COMPLEX [†]	4.74±.01	.303±.001	220±2.3	.216±.001	.330±.002	.482±.001	3.0M
COMPLEX-MOS [†]	4.71±.01	.301±.001	221±1.4	.218±.001	.329±.002	.467±.001	3.3M
RESCAL	4.79±.01	.285±.001	246±2.3	.210±.001	.309±.001	.432±.001	21.9M
RESCAL-MOS	4.65±.01	.318±.001	220±1.1	.230±.002	.348±.001	.494±.001	22.2M
CONVE	4.48±.01	.321±.001	176±2.6	.232±.000	.351±.001	.499±.001	5.1M
CONVE-MOS	4.57±.01	.311±.002	203±1.1	.227±.002	.339±.003	.479±.002	5.4M
COMPGCN	4.80±.07	.300±.005	250±19.8	.215±.004	.328±.005	.474±.008	1.6M
COMPGCN-MOS	4.86±.03	.310±.001	223±5.8	.222±.001	.339±.001	.486±.001	2.0M
<i>d</i> = 1000							
DISTMULT	4.56±.01	.331±.001	208±2.8	.241±.001	.362±.001	.514±.003	15.0M
DISTMULT-MOS	4.72±.00	.311±.001	231±2.3	.221±.003	.341±.000	.492±.002	23.0M
COMPLEX [†]	4.71±.45	.317±.027	224±72.7	.231±.019	.347±.031	.491±.047	15.0M
COMPLEX-MOS [†]	4.64±.00	.314±.001	226±3.1	.225±.001	.343±.001	.497±.001	23.0M
RESCAL	4.64±.00	.307±.001	216±0.7	.221±.001	.335±.003	.483±.002	488.5M
RESCAL-MOS	4.63±.01	.325±.002	259±5.4	.236±.004	.357±.002	.505±.001	496.5M
CONVE	4.65±.04	.301±.001	185±4.3	.212±.001	.329±.001	.485±.002	70.1M
CONVE-MOS	4.69±.01	.316±.001	222±1.5	.227±.001	.347±.001	.497±.002	78.2M

[†] Results for COMPLEX use halved embedding sizes *d* = 100 and *d* = 500.

Table 10: Full results for the Hetionet dataset.

Model	Hetonet						
	NLL↓	MRR↑	MR↓	Hits@1↑	Hits@3↑	Hits@10↑	Param
<i>d</i> = 200							
DISTMULT	6.10±.00	.250±.001	695±2.4	.176±.001	.274±.001	.395±.001	9.0M
DISTMULT-MOS	5.83±.00	.277±.002	488±1.3	.202±.003	.303±.002	.423±.002	9.4M
COMPLEX [†]	6.10±.00	.249±.001	698±2.8	.174±.001	.274±.001	.395±.000	9.0M
COMPLEX-MOS [†]	5.85±.00	.269±.001	500±2.9	.194±.001	.294±.001	.415±.001	9.4M
RESCAL	6.13±.00	.219±.001	607±0.4	.153±.001	.237±.001	.351±.001	10.9M
RESCAL-MOS	5.87±.01	.274±.000	505±2.0	.200±.000	.300±.001	.419±.001	11.3M
CONVE	6.03±.00	.252±.001	610±2.3	.180±.001	.275±.002	.395±.002	11.1M
CONVE-MOS	5.92±.00	.263±.001	536±1.1	.193±.002	.284±.002	.400±.001	11.4M
COMPGCN	5.95±.01	.260±.005	542±3.4	.185±.005	.285±.006	.409±.006	4.7M
COMPGCN-MOS	5.86±.08	.266±.012	484±16.0	.191±.010	.292±.015	.414±.018	5.0M
<i>d</i> = 1000							
DISTMULT	6.04±.00	.288±.000	633±1.9	.217±.001	.314±.000	.429±.000	45.2M
DISTMULT-MOS	5.76±.00	.312±.001	491±1.5	.233±.001	.344±.001	.467±.001	53.2M
COMPLEX [†]	5.99±.00	.292±.000	658±1.8	.219±.001	.320±.000	.437±.000	45.2M
COMPLEX-MOS [†]	5.78±.00	.303±.000	504±2.1	.223±.001	.335±.001	.459±.001	53.2M
RESCAL	5.93±.00	.243±.001	650±3.6	.165±.001	.270±.001	.398±.001	93.1M
RESCAL-MOS	5.87±.03	.300±.009	542±4.9	.223±.009	.327±.010	.454±.008	101.2M
CONVE	6.06±.00	.262±.001	635±4.7	.187±.001	.288±.001	.411±.001	100.3M
CONVE-MOS	5.71±.01	.313±.001	505±3.7	.237±.002	.343±.001	.462±.001	108.3M

[†] Results for COMPLEX use halved embedding sizes *d* = 100 and *d* = 500.

Table 11: Full results for the ogbl-biokg dataset.

Model	ogbl-biokg						
	NLL↓	MRR↑	MR↓	Hits@1↑	Hits@3↑	Hits@10↑	Param
<i>d</i> = 200							
DISTMULT	4.83±.01	.792±.001	5.60±0.1	.713±.001	.849±.001	.935±.001	18.8M
DISTMULT-MOS	4.65±.00	.792±.001	5.32±0.0	.716±.002	.844±.000	.930±.000	19.1M
COMPLEX [†]	4.83±.01	.792±.001	5.56±0.0	.713±.002	.849±.001	.935±.000	18.8M
COMPLEX-MOS [†]	4.65±.00	.793±.001	5.26±0.0	.717±.002	.845±.001	.931±.000	19.1M
RESCAL	4.89±.00	.763±.001	6.01±0.0	.679±.001	.818±.001	.917±.000	22.8M
RESCAL-MOS	4.70±.00	.780±.001	5.47±0.0	.699±.001	.835±.001	.928±.000	23.2M
CONVE	4.94±.00	.782±.001	5.57±0.0	.701±.002	.838±.001	.928±.000	20.8M
CONVE-MOS	4.77±.01	.768±.002	5.77±0.1	.683±.003	.824±.002	.923±.001	21.2M
COMPGCN [‡]	5.11±.20	.749±.019	7.00±0.7	.665±.021	.801±.019	.905±.012	9.5M
COMPGCN-MOS [‡]	4.96±.15	.744±.022	6.93±0.9	.659±.025	.799±.022	.904±.014	9.6M
<i>d</i> = 1000							
DISTMULT	4.89±.02	.801±.002	5.96±0.1	.726±.003	.855±.002	.936±.001	93.9M
DISTMULT-MOS	4.34±.00	.837±.001	4.51±0.0	.772±.002	.884±.000	.951±.000	101.9M
COMPLEX [†]	4.86±.00	.806±.001	5.49±0.0	.731±.002	.860±.001	.940±.000	93.9M
COMPLEX-MOS [†]	4.39±.00	.836±.001	4.50±0.0	.770±.001	.883±.000	.951±.000	101.9M
RESCAL	4.74±.00	.799±.001	5.66±0.0	.723±.001	.851±.000	.939±.000	195.8M
RESCAL-MOS	4.42±.01	.824±.004	4.87±0.1	.755±.005	.874±.002	.947±.001	203.8M
CONVE	4.93±.00	.807±.000	5.25±0.0	.731±.001	.863±.000	.941±.000	149.0M
CONVE-MOS	4.43±.00	.817±.001	5.17±0.1	.744±.001	.872±.000	.946±.000	157.0M

[†] Results for COMPLEX use halved embedding sizes *d* = 100 and *d* = 500.

[‡] Results for COMPGCN use *d* = 100 due to computational constraints.

Table 12: Full results for the openbiolink dataset.

Model	openbiolink						
	NLL↓	MRR↑	MR↓	Hits@1↑	Hits@3↑	Hits@10↑	Param
<i>d</i> = 200							
DISTMULT	5.14±.00	.302±.002	1120±10.6	.195±.004	.342±.000	.530±.000	36.2M
DISTMULT-MOS	5.03±.01	.314±.001	966±33.4	.207±.001	.351±.001	.543±.000	36.5M
COMPLEX [†]	5.13±.01	.301±.001	1200±20.2	.193±.002	.340±.001	.530±.001	36.2M
COMPLEX-MOS [†]	5.06±.00	.313±.002	909±18.5	.206±.003	.350±.002	.539±.004	36.5M
RESCAL	5.16±.00	.303±.001	960±2.20	.197±.002	.339±.001	.527±.001	38.4M
RESCAL-MOS	5.04±.01	.323±.005	949±78.8	.217±.004	.361±.005	.547±.005	38.8M
CONVE	5.28±.02	.286±.000	794±17.6	.181±.001	.320±.002	.509±.002	38.3M
CONVE-MOS	5.10±.01	.304±.002	967±47.9	.200±.002	.340±.003	.528±.002	38.6M
COMPGCN [‡]	5.43±.07	.263±.007	573±27.0	.162±.005	.293±.009	.480±.012	18.3M
COMPGCN-MOS [‡]	5.35±.06	.278±.001	515±35.9	.174±.003	.312±.004	.495±.009	18.3M
<i>d</i> = 1000							
DISTMULT	5.17±.02	.316±.004	1210±21.2	.209±.004	.357±.003	.541±.004	181.0M
DISTMULT-MOS	4.89±.01	.347±.000	799±32.1	.236±.002	.392±.002	.579±.002	189.0M
COMPLEX [†]	5.12±.01	.322±.001	1230±33.9	.213±.001	.364±.002	.550±.001	181.0M
COMPLEX-MOS [†]	4.87±.01	.345±.001	725±18.7	.235±.002	.388±.001	.575±.001	189.0M
RESCAL	5.03±.00	.328±.002	1330±26.6	.222±.002	.366±.001	.552±.002	237.0M
RESCAL-MOS	5.00±.01	.330±.003	1210±27.8	.220±.003	.373±.003	.559±.004	245.0M
CONVE	5.24±.00	.308±.001	1140±24.2	.201±.001	.348±.001	.535±.001	236.2M
CONVE-MOS	4.91±.01	.336±.000	881±22.4	.227±.001	.378±.000	.565±.001	244.2M

[†] Results for COMPLEX use halved embedding sizes *d* = 100 and *d* = 500.

[‡] Results for COMPGCN use *d* = 50.

Table 13: Full results for the WN18RR dataset.

Model	WN18RR						
	NLL↓	MRR↑	MR↓	Hits@1↑	Hits@3↑	Hits@10↑	Param
<i>d</i> = 200							
DISTMULT	6.73±.02	.421±.001	7220±2.5	.397±.002	.429±.001	.469±.001	8.2M
DISTMULT-MOS	9.08±.79	.129±.154	8080±2000	.107±.152	.134±.159	.171±.157	8.6M
COMPLEX [†]	6.04±.04	.436±.001	7640±347	.413±.002	.446±.001	.479±.001	8.2M
COMPLEX-MOS [†]	8.67±.38	.143±.067	7590±563	.112±.062	.153±.071	.202±.074	8.6M
RESCAL	8.66±.54	.215±.113	7640±2010	.187±.116	.225±.112	.267±.104	9.1M
RESCAL-Mos	8.91±.56	.139±.137	7630±1730	.112±.130	.146±.145	.188±.148	9.4M
CONVE	7.31±.03	.230±.002	4300±265	.177±.003	.250±.002	.327±.004	10.3M
CONVE-Mos	8.54±.41	.116±.071	5610±1390	.078±.056	.127±.081	.189±.102	10.6M
COMPGCN	7.38±.13	.411±.002	4550±167	.386±.002	.418±.002	.459±.002	4.2M
COMPGCN-Mos	9.04±.04	.396±.001	5250±120	.379±.002	.402±.001	.428±.003	4.6M
<i>d</i> = 1000							
DISTMULT	6.44±.01	.438±.001	6380±70.9	.405±.001	.449±.002	.507±.002	41.1M
DISTMULT-MOS	6.02±.02	.435±.002	5650±106	.413±.002	.443±.002	.477±.002	49.2M
COMPLEX [†]	5.67±.02	.460±.001	6970±187	.429±.001	.475±.001	.520±.001	41.1M
COMPLEX-MOS [†]	5.93±.17	.439±.003	5310±63.7	.417±.001	.446±.004	.481±.008	49.2M
RESCAL	8.14±.96	.378±.020	5750±960	.357±.018	.387±.021	.417±.023	63.1M
RESCAL-Mos	6.79±1.58	.421±.028	4820±175	.394±.032	.433±.024	.469±.024	71.1M
CONVE	5.55±.01	.433±.001	3860±25.2	.394±.001	.448±.001	.511±.002	96.2M
CONVE-Mos	7.26±.15	.416±.010	4400±62.3	.391±.012	.427±.009	.462±.009	104.3M

[†] Results for COMPLEX use halved embedding sizes *d* = 100 and *d* = 500.